



OPEN ACCESS

EDITED BY

Xixin Wang,
Yangtze University, China

REVIEWED BY

Ruiliang Guo,
Xi'an Shiyou University, China
Ximeng Wang,
Texas A&M University, United States
Tao Hu,
China University of Petroleum, China

*CORRESPONDENCE

Zhengjian Xu,
✉ xumou08@sina.com

RECEIVED 20 March 2024

ACCEPTED 30 April 2024

PUBLISHED 13 June 2024

CITATION

Wang T, Xu Z, Yuan K, Wang X and Ge M (2024), Paleoenvironment and shale gas potential of the Carboniferous Dawuba and the Cambrian Niutitang shales in the Upper Yangtze Platform, South China. *Front. Earth Sci.* 12:1404178. doi: 10.3389/feart.2024.1404178

COPYRIGHT

© 2024 Wang, Xu, Yuan, Wang and Ge. This is an open-access article distributed under the terms of the [Creative Commons Attribution License \(CC BY\)](https://creativecommons.org/licenses/by/4.0/). The use, distribution or reproduction in other forums is permitted, provided the original author(s) and the copyright owner(s) are credited and that the original publication in this journal is cited, in accordance with accepted academic practice. No use, distribution or reproduction is permitted which does not comply with these terms.

Paleoenvironment and shale gas potential of the Carboniferous Dawuba and the Cambrian Niutitang shales in the Upper Yangtze Platform, South China

Ting Wang^{1,2,3}, Zhengjian Xu^{4,5,6,7*}, Kun Yuan^{2,3,8}, Xunlian Wang¹ and Mingna Ge^{2,3,8}

¹School of Earth Sciences and Resources, China University of Geosciences (Beijing), Beijing, China, ²Oil and Gas Survey, China Geological Survey, Ministry of Natural Resources, Beijing, China, ³The Key Laboratory of Unconventional Oil and Gas, China Geological Survey, Beijing, China, ⁴School of Petroleum Engineering, Chongqing University of Science and Technology, Chongqing, China, ⁵Chongqing Institute of Geology and Mineral Resources, Chongqing, China, ⁶Key Laboratory of Tectonics and Petroleum Resources (China University of Geosciences), Ministry of Education, Wuhan, China, ⁷Key Laboratory of Sedimentary Basin and Oil and Gas Resources, Ministry of Natural Resources, Chengdu, China, ⁸School of Energy Resources, China University of Geosciences (Beijing), Beijing, China

Marine shale gas has emerged as a prominent unconventional petroleum resource in recent years, known for its abundant reserves and energy potential. Based on the database of geochemical, mineralogy and physical lab measurements, this study investigates the paleoenvironmental conditions and shale gas potential of the Carboniferous Dawuba and Cambrian Niutitang shales in the Upper Yangtze Platform, South China. Analysis of the paleoclimate and water conditions reveals that the Dawuba shale was deposited under a warm and arid climate with reducing conditions that favored organic matter (OM) preservation, transitioning towards marine conditions with increasing salinity. The Niutitang shale experienced a cooler, arid climate with prevalent saltwater and reducing conditions, also conducive to OM preservation. Both formations have reached the post-mature stage, displaying good to excellent source rock potential. The Dawuba shales are characterized by Type II₂ kerogens, while the Niutitang shales predominantly contain Type I kerogens, indicating high gas generation potentials for both. The formations are composed of mixed and argillaceous shales, exhibiting ultra-low porosity and permeability but featuring development of dissolution pores, OM pores, and micro-fractures essential for gas storage. Comparative analysis shows the Dawuba shales have superior BET-specific surface areas, total pore volumes, and average pore diameters than the Niutitang shales. However, gas contents in both formations are relatively low, underscoring the necessity for further research on shale gas preservation conditions. The Qiannan Depression in Guizhou, particularly the Shangyuan and Zongdi areas of the Dawuba Formation, are identified as promising regions for shale gas exploration due to favorable geological characteristics. This study

highlights the significant shale gas potential in the Upper Yangtze Platform and calls for focused research to optimize exploration and extraction efforts.

KEYWORDS

paleoenvironment, Carboniferous Dawuba Formation, Cambrian Niutitang Formation, Upper Yangtze Platform, shale gas potential

1 Introduction

Mudrocks, encompassing sedimentary rocks such as shale, claystone, mudstone, and siltstone, are characterized by particles smaller than 62.5 μm and constitute more than 50% of sedimentary rock types (Milliken, 2014; Wang X. X. et al., 2019; Xu et al., 2019; Xu Z. J. et al., 2022; Xu Z. J. et al., 2022; Hu et al., 2022; Wang and Cheng, 2023; Wang et al., 2023). While “shale” is sometimes narrowly defined to describe visibly laminated, fissile varieties of sedimentary rock, this research adopts a broader application of the term. Here, “shale” refers to the entire class of fine-grained layered sedimentary rocks, and the term is used interchangeably with “mudrock” where appropriate (Boggs, 2006). Notably, shale represents a significant portion of the Earth’s depositional record, accounting for approximately two-thirds, and covers a quarter of the continental landmass (Garrels and Mackenzie, 1969; Blatt, 1982; Jin et al., 2014).

Shale gas, the leading unconventional petroleum resource, is generated and stored in fine-grained shale, which serves as both the source rock and reservoir in the gas shale system. Shale gas is primarily found in the absorbed phase on clay and organic matter (OM) surfaces, the free phase within pore spaces and fractures, and in low abundance as the dissolved phase in residual hydrocarbons or water, and produced by horizontal drilling and multi-stage hydraulic fracturing (Curtis, 2002; Jarvie et al., 2007). In China, organic-rich shales have been identified in diverse sedimentary environments, including marine (the Silurian Longmaxi Formation shale in the Sichuan Basin), lacustrine (the Cretaceous Qingshankou Formation shale in the Songliao Basin), and transitional environments (the Permian Shanxi Formation shale in the Ordos Basin) (Zou et al., 2022).

Since the year 2000, global shale gas production has seen a steady increase, reaching 840 \times 10⁹ m³ in 2022 and comprising 20.9% of the world’s natural gas production. The United States, benefiting from advancements in hydraulic fracturing technology, reported a significant contribution of 795 \times 10⁹ m³ to its natural gas production in 2022, representing 73% of the national total. Meanwhile, shale gas production in China, commencing in 2012, has reached over 25 \times 10⁹ m³ by 2023, accounting for 10.7% of its natural gas output. Noteworthy industrial breakthroughs in shale gas exploration and development within China have predominantly occurred in the marine shales of the Ordovician Wufeng and the Silurian Longmaxi Formations in Weiyuan, Zhaotong, Jiaoshiba, and Fuling areas in Sichuan Basin (Li et al., 2015; Wu et al., 2016; Yuan et al., 2018; Zhang, 2019; Ge et al., 2020; Wang, 2020; Yang et al., 2021; Ge et al., 2024).

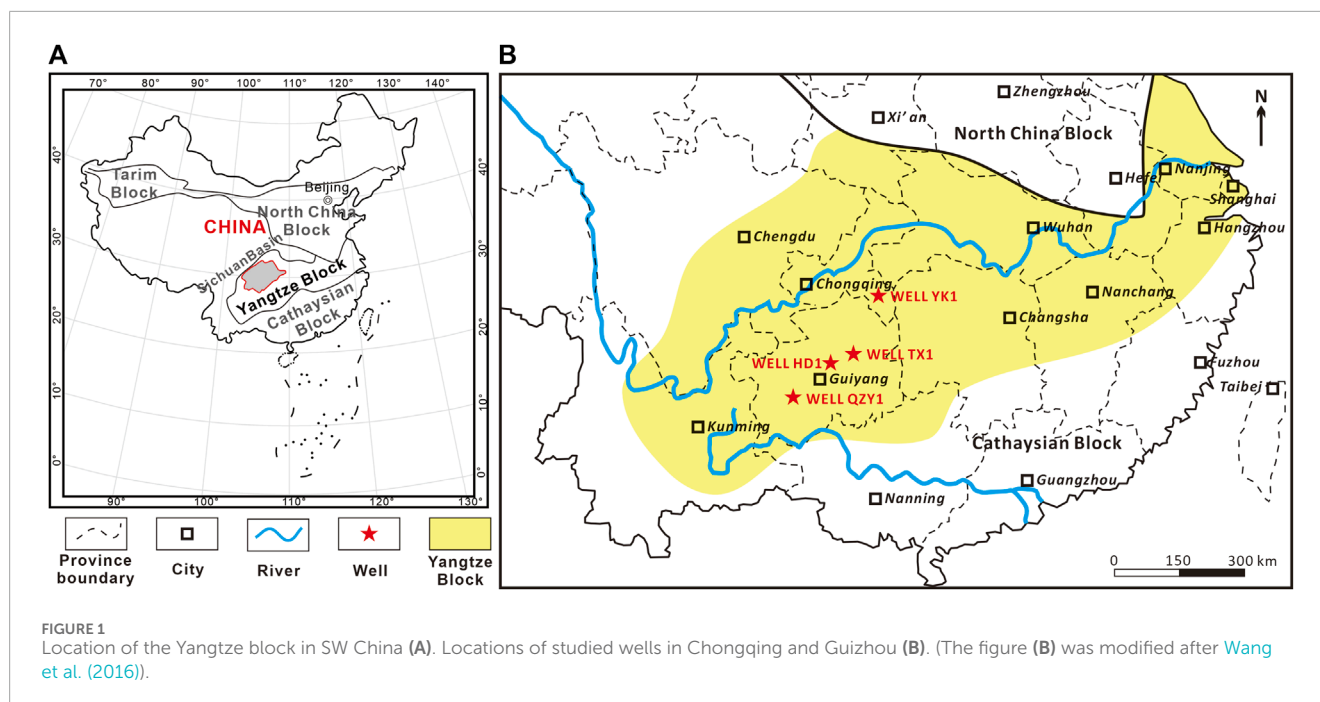
As shale gas development and production progress in the Sichuan Basin, it is crucial to prioritize the selection of new target layers and favorable zones. In 2023, Well Z201, tapped into the Cambrian Qiongzhusi Formation in the Southern Sichuan Basin,

demonstrated the productivity potential of the region, with a single-well shale gas output reaching 73.88 \times 10⁴ m³ per day. The Qiongzhusi shale is geologically equivalent to the Niutitang shale found in the Chongqing and Guizhou areas. Field investigations and drilling activities have indicated that the Cambrian Niutitang Formation and the Carboniferous Dawuba Formation, hereafter referred to as Niutitang and Dawuba shales, in Guizhou and Chongqing are promising strategic exploration zones for marine shale gas on the periphery of the Sichuan Basin (Li et al., 2015; Wu et al., 2016; Yuan et al., 2018; Zhang, 2019; Ge et al., 2020; Wang, 2020; Yang et al., 2021; Ge et al., 2024). These formations feature thick shale layers, up to 200 m, making them primary targets for further exploration (Li et al., 2015; Wu et al., 2016; Yuan et al., 2018; Zhang, 2019; Ge et al., 2020; Wang, 2020; Yang et al., 2021; Ge et al., 2024). Additionally, these shales are characterized by relatively high OM abundance and thermal maturity, which are critical factors for successful shale gas extraction. However, the geological settings in Guizhou and Chongqing are more complex compared to the central Sichuan Basin. These regions have experienced multi-stage tectonic evolution, prolonged periods of uplifting, the presence of numerous faults, and higher levels of OM thermal maturity (Li et al., 2015; Wu et al., 2016; Yuan et al., 2018; Zhang, 2019; Ge et al., 2020; Wang, 2020; Yang et al., 2021; Ge et al., 2024). Such complexity poses significant challenges for shale gas exploration. Consequently, there is a pressing need for more comprehensive studies focusing on source rocks and reservoir characteristics to better understand and exploit these resources effectively.

This research aims to analyze the shales within the Cambrian Niutitang Formation and Carboniferous Dawuba Formation in Guizhou and Chongqing, situated in the Upper Yangtze Platform. The study’s objectives include reconstructing the paleoenvironments, evaluating source rock characteristics, shale reservoir properties, and gas content to offer insights into the shale gas potential of the Cambrian and Carboniferous periods in the Upper Yangtze Platform. These findings are intended to guide unconventional hydrocarbon exploration efforts in analogous regions.

2 Geological settings

The Upper Yangtze Platform, situated in the western part of the Yangtze Platform in South China, encompasses a vast area including eastern Sichuan, the Chongqing area, the majority of Guizhou, western parts of Hubei and Hunan, and northern Yunnan province (Tan et al., 2013) (Figure 1). Notably, southeastern Chongqing, geographically positioned within the eastern Sichuan Basin, plays a pivotal role in the Upper Yangtze plate due to its location in the transitional zone between the Central Sichuan Uplift and the Central Guizhou Uplift (Li et al., 2015; Wu et al., 2016;



Zhang, 2019; Wang, 2020). Further south, the Qiannan Depression in South Guizhou Province is encircled by significant geological features: the Guiyang-Zhenyuan fault zone and the Qianzhong uplift to the northwest, the Tongren-Sandu fault zone and the Xuefengshan uplift to the east and southeast, and the Ziyun-Luodian fault zone to the southwest (Wu et al., 2012; Lu, 2019).

During the Ediacaran-Cambrian transition, the Yangtze Block, bordered by two narrow margin-slope zones along the northern and south-southwest flanks (Chen et al., 2009), experienced significant geological changes influenced by global continental rearrangements. Specifically, these changes included the rifting of Laurentia from western Gondwana (Meert, 2003) and the simultaneous amalgamation of Australia with East Antarctica and eastern Gondwana, which coincided with the collision between East and West Gondwana (Kirschvink, 1992; Meert, 2003). These tectonic events indirectly influenced sedimentation patterns on the Yangtze Platform (Goldberg et al., 2007). At this time, much of the Yangtze Block was covered by extensive carbonate platforms. These platforms were subsequently submerged by a deep muddy shelf system at the onset of the Early Cambrian, a result of a global marine transgression known as the “Niutitang Event” (Steiner et al., 2001). This significant marine transgression during the early Cambrian period led to the widespread deposition of thick black shales in restricted marine environments across the region (Li et al., 2015; Wu et al., 2016; Zhang, 2019; Wang, 2020). The Upper Yangtze Platform functioned as a pericontinental marine shelf during this period. It was bordered by a paleocontinent to the west and featured a gradient of depositional environments extending southeastward. This gradient included a marine platform, a restricted marine basin, a former island arc system, and a deep marine setting (Tan et al., 2014; Tan et al., 2015). The early Cambrian shales of the Niutitang Formation (also known as the Qiongzhusi Formation shales or Jiulaodong Formation shales in the southwestern part of the Sichuan Basin) consisted of lower siliceous successions and

upper black shale successions. These formations were extensively deposited around the northern and southern flanks of the Yangtze Platform, establishing the Lower Cambrian black shales as one of the principal source rocks and shale gas reservoirs on the Upper Yangtze Platform.

The Early Carboniferous was a pivotal period marked by the transition from the mid-Paleozoic greenhouse climate to the Late Paleozoic Ice Age. This interval featured two short glaciation events during the mid-Tournaisian and Viséan stages, which were consistent with frequent global sea-level changes (Kaiser et al., 2011; Lakin et al., 2016; Liu et al., 2019; Qie et al., 2019). Concurrently, the Carboniferous Period was characterized by intense global tectonic activity, notably including strong rifting in the Qiannan Depression of the South China (Wang X. D. et al., 2019; Wang Q. F. et al., 2020). During the late Middle Devonian to early Late Devonian, the extent of marine transgression was at its peak, leading to the formation of a chert-siliceous mudstone assemblage (Wang et al., 2006). This transgressive phase slightly receded in the early Early Carboniferous but resumed in the middle Early Carboniferous. This subsequent transgression resulted in the formation of a parallel unconformity within the Datangian strata across various ages, leading to the deposition of a distinctive shale-chert-limestone sedimentary assemblage (Guizhou Geological Survey Institute, 2017). The Lower Carboniferous Dawuba Formation, primarily located in the Luodian, Wangmo, and Ziyun areas of Guizhou, is a notable geological unit from this period. It consists of Datangian slope-basin facies shales interbedded with chert and limestone, stratigraphically positioned above the Muhua Formation limestone and below the limestone of the Nandan Formations (Guizhou Geological Survey Institute, 2017). Characterized by a thickness of approximately 150–250 m, the Dawuba Formation includes shale, silty shale, siltstone, and sandstone, indicative of deposition in an offshore delta (Yuan et al., 2018; Lu, 2019). This formation is further divided stratigraphically into four members,

from the first to the fourth member, arranged sequentially from the bottom to the top. Exploration efforts, including the drilling of three exploratory wells, have established the Dawuba Formation as a significant target for shale gas exploration in the Qiannan Depression of the South China (Yuan et al., 2018). Notably, the shales within this formation are identified as the primary source rocks for gas, distinguished by their high OM abundance and thermal maturity. Additionally, these shales also serve as direct cap rocks for the gas reservoirs, enhancing their significance in hydrocarbon exploration.

3 Data and methods

3.1 Samples and data

The collection and analysis of Dawuba Shale samples were comprehensively conducted from Well QZY1, encompassing a variety of tests to assess the shale's characteristics. A structured approach was applied in sample collection and analysis, with a total of 45 samples designated for major element analysis and 35 samples for trace element analysis. To understand the organic composition, 25 samples underwent organic petrographic characterization, and 26 samples were analyzed for vitrinite reflectance (Ro%). The total organic carbon (TOC) content was determined from 33 samples. For mineralogical composition, 60 samples were subjected to X-ray diffraction (XRD) analysis. Additionally, the study included physical property assessments on six core plug samples and gas content analysis on 16 samples. Preparation of samples varied according to the analysis requirements, with polished sections being prepared for organic petrology and vitrinite reflectance analysis, while other samples were processed into powders for various chemical analyses.

In the case of the Niutitang shales within the Guizhou area, samples and data were obtained from Well HD1, complemented by research findings from Ge et al. (2020, 2024) (Ge et al., 2020; Ge et al., 2024) and Yang et al. (2021) (Yang et al., 2021). For the Niutitang shales in the Chongqing area, data were sourced from studies by Li et al. (2015) (Li et al., 2015), Wu et al. (2016) (Wu et al., 2016), Zhang (2019) (Zhang, 2019), and Wang (2020) (Wang, 2020). This diverse dataset, combining direct sample analysis with insights from recent studies, provides a robust foundation for evaluating the geochemical, petrographic, and gas potential of these shale formations.

3.2 Methods

No unexpected or unusually high safety hazards were encountered during the testing.

3.2.1 Methods for major and trace element analysis

The preparation of samples for major and trace element analysis involved a meticulous process. Initially, the samples were pulverized to a fine consistency of about 200 mesh. Subsequently, they were dried at 105 °C for 4 h to eliminate moisture, and then allowed to cool to room temperature, approximately 23°C, in a desiccator to

prevent moisture reabsorption. For determining the concentrations of major elements, X-ray Fluorescence Spectrometry (XRF) was employed. The preparation of fused glass beads, essential for the XRF analysis, adhered to the procedure outlined by Couture et al. (1993) (Couture et al., 1993). Additionally, the loss on ignition (LOI), which quantifies the amount of material lost upon heating, was measured gravimetrically at a temperature of about 1,100°C. The detection of trace element concentrations was facilitated by Inductively Coupled Plasma-Mass Spectrometry (ICP-MS) following the dissolution of the solid samples. This step was guided by the protocols of the Chinese National Standard GB/T14506.30-2010, utilizing a screw-top Teflon bomb with an aqueous HF-HNO₃ mixture for dissolution (Jenner et al., 1990).

3.2.2 Methods for source rock characterization

The characterization of source rocks commenced with the preparation of polished sections for organic petrological analysis. Kerogen, the insoluble OM in sedimentary rocks, was extracted through a meticulous process that involved the successive removal of soluble OM, mineral matter, and water from the shale samples (Durand et al., 1980; Suleimenova et al., 2014). The isolated kerogen was then thinly sliced and mounted for microscopic examination. The composition of macerals within the kerogen was assessed using a Leica MPV Compact II microscope, capable of both reflected white and fluorescent light imaging. Additionally, vitrinite reflectance (Ro%), a key indicator of thermal maturity, was measured with the same microscope model, equipped with a micro-photometer and an oil immersion lens (Zeng et al., 2013; Ayinla et al., 2017). Calibration of these measurements was achieved using a standard reflectance value of 1.78% for the GGG standard (gallium-gadolinium-garnet), with results captured via DISKUS software (Ayinla et al., 2017).

For the determination of Total Organic Carbon (TOC), the samples underwent grinding to a particle size of less than 200 mesh and were then pre-treated with a 5% HCl solution at 80°C to eliminate carbonates (Espitalie et al., 1977; Tissot and Welte, 1984; Peters et al., 1994). The TOC content was quantified using a LECO elemental analyzer, providing a comprehensive overview of the organic carbon present within the samples.

3.2.3 Methods for reservoir bed characterization

The characterization of reservoir beds in the Dawuba and Niutitang shales involved a series of meticulously designed experiments to assess their mineral composition, porosity, permeability, pore morphology, and gas content.

3.3 Mineral composition analysis

For mineral content and clay composition, X-ray diffraction analysis (XRD) was conducted on crushed samples (200 mesh). Utilizing a Bruker D8 Advance XRD system with Cu-K α radiation at 40 kV voltage and 40 mA current, this analysis semi-quantified the mineral constituents of the shales.

3.4 Porosity and permeability measurements

Porosity was determined using the CMS-300 instrument on core plugs at a pressure of 200 psi, providing insights into the storage capacity of the shales. Air permeability was assessed with a pulse-decay permeameter at a mean gas pressure of 435 psi (3 MPa), offering information on the ease with which gases can flow through the shale matrix.

3.5 Pore morphology characterization

Scanning electron microscopy (SEM) was employed to examine the pore morphology on freshly broken surfaces of the shales. Samples were coated with a gold/palladium (Au/Pd) alloy and observed under a Tescan Vega 3 LM system. The SEM operated at a high vacuum with 20 kV acceleration voltages and electric detectors, achieving a maximum resolution of 3 nm.

3.6 Pore characterization through low-pressure N₂-physisorption

Low-pressure N₂-physisorption tests were performed using a Micromeritics ASAP 2020 apparatus to characterize the pores within the shales. Crushed samples (60–80 mesh) were outgassed overnight at 110°C under vacuum to eliminate volatile substances and moisture. The N₂ adsorption/desorption isotherms were then recorded at 77 K. Analysis of the adsorption data employed non-local density functional theory (NLDFT) and multipoint Brunauer–Emmett–Teller (BET) analyses for specific surface area (SSA), along with Barrett–Joyner–Halenda (BJH) analysis for pore size distribution (PSD), as detailed by Sing (1995), Lowell et al. (2004), and Barrett et al. (1951) (Barrett et al., 1951; Sing, 1995; Lowell et al., 2004). The pore-size distribution was illustrated using the $dV/d\log(D)$ versus D plot for N₂ adsorption, which effectively highlights the volume distribution of pores.

3.7 Shale gas collection

The collection of shale gas utilized a gas gathering system based on the water gas displacing method, using a saturated salt solution as the displacing medium. Pressure-core samples were immediately placed in an air collector upon extraction from the drilling borehole. The gas collected during the unheated stage was categorized as desorbed gas. After reaching a plateau in desorbed gas collection, the system was heated to gather residual gas. The quantification of lost gas was not included in this study.

4 Depositional environments of shale layers

The characterization of depositional environments in shale layers involves analyzing the composition and concentration of major and trace elements within the samples. The major elements, presented as oxides, include SiO₂, Al₂O₃, and CaO, which dominate the samples. In contrast, Fe₂O₃, MgO, K₂O, and SO₃ are found in relatively lower abundances (Table 1). Additionally, trace elements such as sodium oxide (Na₂O), manganese oxide (MnO), titanium dioxide (TiO₂), vanadium pentoxide (V₂O₅), chromium oxide (Cr₂O₃), barium oxide (BaO), and phosphorus pentoxide (P₂O₅) are present but in concentrations below 1%. Notably, the silica (SiO₂) content in the samples varies significantly, ranging from 2.86% to 69.31%, with an average of 45.98%. This average is lower than the typical shale content of 58.9% reported by Wedepohl (1971) (Wedepohl, 1971). The SiO₂/Al₂O₃ ratio further highlights this variance, ranging from 2.38 to 14.68, with an average of 3.71, slightly higher than the average for typical shale (AS, 3.53). A comparative analysis reveals that the Dawuba shales are enriched in elements such as Be, Cr, Ni, Mo, Ba, and U, yet exhibit depletion in Li, Cu, and Zn when compared to AS, with the remaining trace elements showing similar concentrations to AS (Table 2).

4.1 Paleoclimate

The composition of major and trace elements, alongside their ratios, serves as a robust proxy for understanding the depositional environments of detrital sediments. These proxies offer valuable insights into the paleoclimate, water restriction, redox conditions, and paleoproductivity of the depositional period (Jones and Manning, 1994; Lin et al., 2008; Zeng et al., 2015; Guo et al., 2020). Specifically, the Ga/Rb and Sr/Cu ratios are instrumental in reconstructing paleoclimate conditions. Higher Ga/Rb ratios suggest warmer temperatures and reduced aridity (Lerman and Gat, 1989; Bai et al., 2015), whereas Sr/Cu ratios provide an indication of humidity levels, with values below 10.0 pointing to humid conditions and those above 10.0 suggesting aridity (Adegoke et al., 2014; Sarki Yandoka et al., 2015). Analysis of the Dawuba shales in Guizhou, as depicted in Figures 2, 3A, indicates that they were primarily deposited under conditions that were both warm and arid.

According to the data collected from Li et al. (2015) (Li et al., 2015) and Yang et al. (2021) (Yang et al., 2021), the Niutitang shales from the Chongqing area exhibit Sr/Cu ratios ranging from 1.99 to 17.41, with an average of 6.70, and Ga/Rb ratios between 0.15 and 0.22, averaging at 0.18 (Figure 3B). Similarly, the Niutitang shales from the Guizhou area display Sr/Cu ratios from 1.37 to 25.64, with an average of 4.29 (Figure 3C). These results suggest the prevalence of cooler paleo-conditions during the Cambrian Niutitang deposition.

4.2 Paleosalinity

Understanding paleosalinity, which is a key factor in reconstructing past marine environments, can be approached

TABLE 1 Relative content of the major elements of the Dawuba shales in Guizhou, SW China (Data from Well QZYY1).

No.	Depth/m	Lithology	Contents/%														A
			SiO ₂	Al ₂ O ₃	Fe ₂ O ₃	MgO	CaO	Na ₂ O	K ₂ O	MnO	TiO ₂	V ₂ O ₅	Cr ₂ O ₃	BaO	SO ₃	P ₂ O ₅	
ZY1-YX-1	2668.00	Shale	48.84	15.71	6.23	2.36	10.53	0.33	3.16	0.03	0.66	0.03	0.01	0.08	4.74	0.08	15.02
ZY1-YX-3	2688.00	Shale	49.43	15.57	5.60	2.30	11.21	0.19	3.20	0.03	0.66	0.03	0.02	0.07	3.94	0.05	14.77
ZY1-4-05	2699.00	Shale	54.72	20.94	5.81	2.19	4.39	0.12	4.28	0.02	0.88	0.04	0.02	0.05	2.46	0.06	10.46
ZY1-YX-5	2702.00	Shale	47.97	15.94	6.26	1.65	9.89	0.90	2.21	0.03	0.79	0.03	0.01	0.64	8.26	0.09	10.35
ZY1-YX-76	2709.00	Shale	49.66	16.75	6.14	2.60	9.76	0.33	3.54	0.03	0.67	0.03	0.02	0.17	3.68	0.11	15.52
ZY1-YX-85	2719.00	Shale	47.57	15.07	5.89	2.67	12.23	0.27	3.17	0.03	0.61	0.03	0.01	0.04	4.36	0.06	17.72
ZY1-YX-8	2728.00	Shale	48.35	15.56	6.32	1.68	10.15	0.94	2.10	0.04	0.79	0.03	0.01	0.61	7.76	0.10	10.80
ZY1-YX-9	2738.00	Shale	46.66	12.71	4.81	1.85	14.01	0.78	1.76	0.02	0.64	0.03	0.01	1.04	6.76	0.18	14.56
ZY1-YX-11	2750.00	Shale	47.86	15.48	5.56	3.29	10.70	0.14	3.68	0.02	0.64	0.03	0.02	0.32	3.59	0.07	21.25
ZY1-YX-119	2759.00	Shale	52.30	14.12	7.48	2.02	8.77	0.73	2.32	0.04	0.64	0.03	0.01	0.93	6.01	0.15	14.31
ZY1-YX-136	2787.00	Shale	61.42	14.60	5.74	1.26	3.45	0.88	1.92	0.02	0.71	0.03	0.01	0.99	7.95	0.21	8.63
ZY1-6-01	2796.00	Shale	63.39	15.79	5.05	1.18	1.64	2.47	2.06	0.01	0.78	0.03	0.01	0.04	5.96	0.04	7.47
ZY1-6-03	2798.20	Shale	59.09	18.09	6.77	1.40	1.37	1.04	2.54	0.02	0.79	0.03	0.02	0.05	8.57	0.05	7.74
ZY1-6-05	2800.50	Shale	59.08	20.75	5.38	1.42	0.48	1.13	2.65	0.01	0.98	0.04	0.02	0.05	7.44	0.04	6.84
ZY1-6-07	2802.60	Shale	60.24	16.66	6.25	1.09	1.97	0.92	2.01	0.01	0.89	0.03	0.02	0.04	9.37	0.22	6.54
ZY1-6-09	2804.70	Shale	56.47	19.30	7.22	1.40	1.31	1.04	2.54	0.01	0.87	0.04	0.02	0.06	9.09	0.08	7.25
ZY1-7-02	2807.55	Shale	57.00	18.98	6.16	1.36	3.14	0.95	2.24	0.01	0.79	0.04	0.02	0.06	8.51	0.08	7.17
ZY1-7-04	2808.50	Shale	67.81	12.82	4.71	1.11	2.02	0.79	1.75	0.01	0.79	0.03	0.01	0.04	6.16	0.12	8.66
ZY1-7-06	2810.50	Shale	57.35	20.24	6.51	1.38	0.64	0.94	2.78	0.02	0.88	0.04	0.02	0.06	8.33	0.06	6.82
ZY1-7-08	2812.50	Shale	64.33	16.10	5.57	0.76	0.37	1.02	1.85	0.01	0.91	0.03	0.02	0.04	8.09	0.10	4.72
ZY1-7-10	2814.50	Shale	58.97	18.23	6.26	1.21	0.87	1.03	2.42	0.01	0.85	0.05	0.02	0.05	9.37	0.10	6.64
ZY1-YX-151	2823.00	Shale	59.89	17.72	5.35	1.39	2.96	1.40	2.31	0.01	0.84	0.04	0.02	0.15	6.99	0.08	7.84

(Continued on the following page)

TABLE 1 (Continued) Relative content of the major elements of the Dawuba shales in Guizhou, SW China (Data from Well QZY1).

No.	Depth/m	Lithology	Contents/%														A
			SiO ₂	Al ₂ O ₃	Fe ₂ O ₃	MgO	CaO	Na ₂ O	K ₂ O	MnO	TiO ₂	V ₂ O ₅	Cr ₂ O ₃	BaO	SO ₃	P ₂ O ₅	
ZY1-YX-25	2828.00	Shale	58.76	10.98	5.80	1.71	9.38	0.59	1.68	0.04	0.53	0.02	0.01	0.38	4.44	0.08	15.57
ZY1-YX-160	2834.00	Shale	56.56	16.68	5.06	1.35	4.19	2.18	2.24	0.01	0.80	0.05	0.02	1.32	7.42	0.07	8.09
ZY1-YX-26	2838.00	Shale	58.64	10.25	6.37	1.80	9.87	0.61	1.52	0.04	0.49	0.02	0.01	0.32	4.37	0.09	17.56
ZY1-YX-172	2847.00	Shale	52.97	15.42	5.15	1.57	8.28	1.90	2.11	0.02	0.72	0.04	0.02	0.46	6.03	0.10	10.18
ZY1-YX-186	2863.00	Shale	38.03	10.97	4.58	3.93	18.12	0.82	1.52	0.03	0.52	0.02	0.01	0.85	6.64	0.07	35.82
ZY1-YX-193	2871.00	Shale	39.32	11.01	4.16	4.01	18.42	0.98	1.53	0.02	0.54	0.02	0.01	1.22	5.63	0.07	36.42
ZY1-8-02	2877.40	Shale	42.48	16.59	7.70	2.06	13.61	0.74	1.84	0.03	0.78	0.03	0.01	0.05	6.26	0.05	12.42
ZY1-8-04	2879.40	Shale	50.85	21.38	5.34	1.56	6.01	1.77	2.85	0.01	1.00	0.04	0.02	0.06	6.55	0.03	7.30
ZY1-8-06	2881.50	Shale	61.44	18.98	4.25	1.40	2.46	1.63	2.73	0.03	0.92	0.03	0.02	0.07	5.13	0.04	7.38
ZY1-8-08	2883.50	Shale	44.44	16.55	5.06	1.68	14.19	0.95	2.28	0.03	0.70	0.03	0.01	0.06	6.83	0.07	10.15
ZY1-8-10	2885.50	Shale	48.00	19.86	5.08	1.71	8.96	1.08	2.70	0.03	0.84	0.03	0.02	0.06	6.37	0.12	8.61
ZY1-9-02	2886.50	Shale	45.35	15.38	4.12	1.32	15.41	0.91	2.07	0.03	0.86	0.03	0.01	0.05	5.95	0.05	8.58
ZY1-9-04	2888.50	Shale	52.51	18.12	4.69	1.18	8.33	1.05	2.60	0.03	0.83	0.03	0.02	0.05	7.69	0.06	6.51
ZY1-9-06	2890.50	Shale	49.77	15.46	4.60	1.26	11.48	0.88	2.09	0.02	0.76	0.03	0.01	0.05	7.44	0.11	8.15
ZY1-9-08	2892.50	Shale	50.24	16.46	4.79	1.17	10.95	0.97	2.26	0.02	0.79	0.03	0.01	0.05	8.23	0.07	7.11
ZY1-9-10	2894.40	Shale	21.32	5.05	1.89	1.63	40.90	0.22	0.58	0.05	0.20	0.01	0.01	0.02	3.27	0.19	32.28
ZY1-YX-206	2903.00	Shale	50.69	18.10	5.46	1.56	7.75	1.64	2.58	0.02	0.83	0.03	0.02	0.31	7.36	0.13	8.62
ZY1-10-2	2927.20	Shale	62.04	12.80	3.20	1.28	5.63	0.78	2.43	0.01	0.51	0.03	0.01	0.11	6.81	0.49	10.00
ZY1-10-7	2931.95	Shale	49.87	17.20	4.76	1.48	9.42	0.64	3.28	0.01	0.80	0.02	0.01	0.15	8.83	0.06	8.60
ZY1-12-5	2950.10	Shale	54.63	18.33	4.88	1.36	5.01	0.52	3.60	0.01	0.79	0.02	0.01	0.15	8.80	0.06	7.42
ZY1-YX-39	2968.00	Shale	45.11	12.52	4.35	1.60	16.34	1.28	2.01	0.02	0.58	0.03	0.02	0.28	5.82	0.08	12.78
ZY1-YX-247	2976.00	Shale	46.39	7.42	2.17	1.62	21.97	0.53	1.21	0.01	0.33	0.03	0.01	0.12	3.69	0.08	21.83
ZY1-13-1	2981.90	Shale	69.31	4.72	1.79	0.75	10.82	0.16	0.95	0.01	0.19	0.03	0.01	0.04	3.28	0.11	15.89

Abbreviations: A, (MgO/Al₂O₃) × 100.

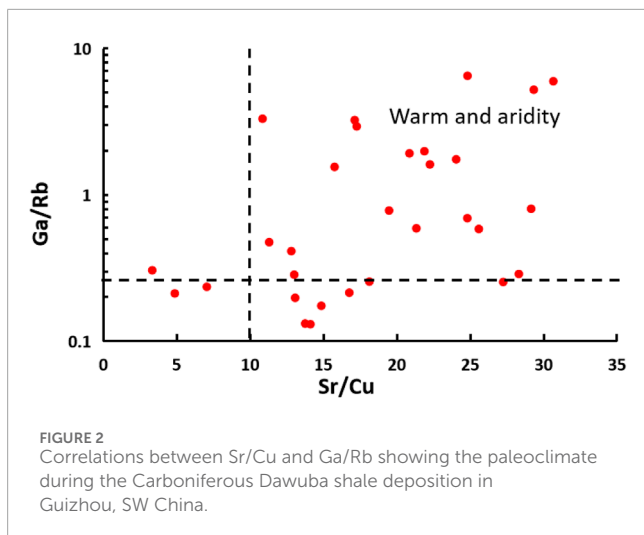
TABLE 2 Contents of the trace elements of the Dawuba shales in Guizhou, SW China (Data from Well QZY1).

No.	Depth/m	Contents (ppm)														Sr/Cu	Ga/Rb	V/(V+Ni)	V/Cr	Ni/Co
		Li	Be	V	Cr	Co	Ni	Cu	Zn	Ga	Rb	Sr	Mo	Pb	U					
ZY1-10-2	2927.20	26.43	1.01	153.20	174.86	8.15	86.30	29.00	95.66	31.25	147.05	7.11	27.46	10.68	4.87	0.21	0.64	0.88	10.59	
ZY1-10-7	2931.95	29.09	1.64	92.95	174.51	12.20	44.62	14.36	58.79	41.60	193.41	0.87	32.31	3.49	16.76	0.22	0.68	0.53	3.66	
ZY1-11-6	2944.10	4.10	0.25	12.00	20.37	2.02	52.31	—	4.08	4.17	6.56	734.60	—	0.38	—	0.64	0.19	0.59	25.90	
ZY1-12-5	2950.10	28.59	1.95	106.29	155.59	12.19	44.69	18.53	73.81	46.24	196.11	0.59	35.50	5.46	7.05	0.24	0.70	0.68	3.67	
ZY1-13-1	2981.90	12.59	0.76	151.58	369.72	7.08	150.31	52.13	134.77	11.19	36.59	31.06	20.10	8.25	3.33	0.31	0.50	0.41	21.23	
ZY1-13-5	2987.00	7.16	0.40	19.13	164.31	2.91	125.94	12.42	35.14	3.56	8.07	6.82	4.65	1.35	—	0.44	0.13	0.12	43.28	
ZY1-4-05	2699.00	115.24	2.62	184.42	127.97	14.83	89.37	19.07	102.52	25.36	191.60	1.66	29.99	3.56	13.75	0.13	0.67	1.44	6.03	
ZY1-YX-1	2668.00	90.45	2.13	146.07	193.54	12.79	80.41	20.42	95.62	27.31	137.71	2.29	32.23	3.35	13.07	0.20	0.64	0.75	6.29	
ZY1-YX-3	2688.00	73.22	1.89	133.83	180.59	10.36	67.75	17.47	60.48	22.93	131.02	1.73	28.53	2.97	14.85	0.18	0.66	0.74	6.54	
ZY1-YX-5	2702.00	154.31	1.87	122.39	170.41	13.06	61.11	16.74	77.57	207.28	104.28	1.40	32.81	3.40	21.88	1.99	0.67	0.72	4.68	
ZY1-YX-8	2728.00	162.82	1.94	130.95	182.84	15.87	67.36	17.39	111.61	198.69	113.54	1.22	36.31	3.51	24.04	1.75	0.66	0.72	4.24	
ZY1-YX-9	2738.00	94.00	1.57	104.26	121.47	9.97	51.88	14.81	80.05	324.53	54.30	1.97	25.37	3.22	30.66	5.98	0.67	0.86	5.20	
ZY1-YX-11	2750.00	37.34	2.08	140.04	120.84	10.71	63.69	18.69	89.99	69.01	145.06	1.19	25.71	3.72	11.30	0.48	0.69	1.16	5.95	
ZY1-YX-16	2770.00	49.63	1.13	78.93	63.75	6.97	53.58	10.43	48.43	20.69	35.33	0.61	15.61	2.56	25.58	0.59	0.60	1.24	7.69	
ZY1-YX-25	2828.00	54.64	1.28	100.56	141.61	8.83	48.60	11.15	60.82	83.29	51.56	248.09	22.56	2.30	22.25	1.62	0.67	0.71	5.50	
ZY1-YX-26	2838.00	51.25	1.23	90.71	90.10	9.58	55.53	12.11	66.61	85.16	44.29	0.55	23.99	2.29	20.86	1.92	0.62	1.01	5.80	
ZY1-YX-28	2858.00	37.23	0.98	39.31	49.43	6.74	60.32	13.30	36.98	25.84	37.24	0.76	13.45	1.47	24.80	0.69	0.39	0.80	8.95	
ZY1-YX-32	2898.00	11.61	0.50	22.00	31.61	3.58	52.24	8.89	15.58	6.89	23.87	0.46	4.25	1.39	28.31	0.29	0.30	0.70	14.59	
ZY1-YX-33	2914.00	11.69	0.49	26.31	29.44	3.41	53.22	13.64	17.34	6.22	24.31	1.11	4.60	1.41	18.12	0.26	0.33	0.89	15.61	
ZY1-YX-36	2938.00	10.85	0.45	23.39	53.31	3.15	49.87	8.88	15.71	5.82	22.89	1.00	3.97	1.57	27.24	0.25	0.32	0.44	15.83	
ZY1-YX-39	2968.00	71.37	1.57	130.16	169.42	8.75	56.49	17.19	105.75	64.17	82.00	6.41	24.41	4.44	19.47	0.78	0.70	0.77	6.46	
ZY1-YX-76	2709.00	70.26	2.06	152.88	189.84	12.22	72.03	18.85	81.53	43.30	151.77	1.64	28.87	3.43	13.01	0.29	0.68	0.81	5.89	

(Continued on the following page)

TABLE 2 (Continued) Contents of the trace elements of the Dawuba shales in Guizhou, SW China (Data from Well QZY1).

No.	Depth/m	Contents (ppm)														Sr/Cu	Ga/Rb	V/(V+Ni)	V/Cr	Ni/Co
		Li	Be	V	Cr	Co	Ni	Cu	Zn	Ga	Rb	Sr	Mo	Pb	U					
ZY1-YX-85	2719.00	64.83	1.88	138.55	136.49	13.23	85.05	19.85	64.27	18.92	144.50	280.09	0.81	30.88	3.20	14.11	0.13	0.62	1.02	6.43
ZY1-YX-119	2759.00	71.85	1.80	128.09	121.41	13.99	72.27	18.14	142.53	293.98	90.60	310.63	0.75	32.07	2.92	17.12	3.24	0.64	1.06	5.17
ZY1-YX-136	2787.00	91.75	1.68	126.23	169.13	10.63	48.43	15.48	95.73	290.40	98.83	267.25	1.81	28.95	3.27	17.26	2.94	0.72	0.75	4.56
ZY1-YX-151	2823.00	133.13	2.17	189.88	202.66	10.36	54.64	16.67	69.75	49.23	119.15	213.48	2.50	31.51	4.13	12.81	0.41	0.78	0.94	5.27
ZY1-YX-160	2834.00	126.86	2.07	213.03	216.75	12.01	70.72	33.27	147.24	407.00	122.83	360.90	6.07	31.47	5.17	10.85	3.31	0.75	0.98	5.89
ZY1-YX-172	2847.00	107.43	1.93	167.04	189.88	9.58	60.27	18.01	116.89	158.89	102.21	283.72	6.88	26.61	4.31	15.75	1.55	0.73	0.88	6.29
ZY1-YX-186	2863.00	68.33	1.35	100.29	102.30	9.02	88.21	14.47	81.59	259.53	49.63	424.37	4.39	22.44	3.79	29.33	5.23	0.53	0.98	9.78
ZY1-YX-193	2871.00	73.72	1.39	110.17	172.19	9.27	57.39	20.09	80.64	345.52	53.09	498.48	3.20	23.75	3.68	24.81	6.51	0.66	0.64	6.19
ZY1-YX-206	2903.00	163.56	2.07	160.46	228.14	12.99	61.67	17.25	93.10	81.36	137.53	367.90	2.88	32.53	3.98	21.33	0.59	0.72	0.70	4.75
ZY1-YX-220	2919.00	20.32	0.40	26.94	99.64	3.42	64.75	4.16	22.63	36.53	12.24	—	2.56	4.18	0.96	—	2.98	0.29	0.27	18.93
ZY1-YX-225	2924.00	22.28	0.42	30.44	84.10	3.66	68.50	4.79	23.44	41.23	14.90	—	2.36	4.40	1.15	—	2.77	0.31	0.36	18.72
ZY1-YX-234	2962.00	10.56	0.32	17.23	41.20	2.79	58.33	3.24	18.82	90.27	9.98	—	1.79	2.48	0.93	—	9.05	0.23	0.42	20.91
ZY1-YX-247	2976.00	37.66	0.80	104.95	100.79	5.42	60.86	12.86	49.39	30.01	37.32	374.84	6.45	13.40	4.45	29.15	0.80	0.63	1.04	11.23



through the analysis of specific elemental ratios and content. The content of molybdenum (Mo) and its ratio to total organic carbon (TOC) are particularly informative. Mo tends to accumulate under anoxic reducing conditions, making its concentration and the Mo/TOC ratio valuable for assessing the degree of water restriction (Algeo and Lyons, 2022). Analysis of the Mo-TOC relationships in the Dawuba shale in Guizhou, particularly within the first member of the Dawuba Formation, suggests sedimentation occurred under conditions of restricted water flow, indicative of an enclosed environment.

Another significant indicator of paleosalinity is the $(\text{MgO}/\text{Al}_2\text{O}_3) \times 100$ ratio. Higher values within this ratio are indicative of increased salinity levels (Wang X. F. et al., 2020). The classification of these ratios into <1 , $1-10$, and >10 correspond to fresh, transitional, and saltwater conditions, respectively. Analysis of the Dawuba shale in Guizhou, as illustrated in Figure 3A, reveals that the depositional environment predominantly ranged from transitional to saltwater. This suggests that during the deposition of the Dawuba shale, the environment transitioned to or was primarily marine.

According to the data collected from Li et al. (2015) (Li et al., 2015) and Yang et al. (2021) (Yang et al., 2021), the $(\text{MgO}/\text{Al}_2\text{O}_3) \times 100$ ratios in the Niutitang shales from the Chongqing area demonstrate a range from 8.74 to 79.49, with an average of 18.72 (Figure 3B). This indicates a predominance of saltwater conditions. Furthermore, the Sr/Ba ratio, another proxy for inferring paleosalinity where higher ratios suggest greater salinity (Meng et al., 2012), supports this conclusion. In the Niutitang shales of the Guizhou area, Sr/Ba ratios range from 1.80 to 9.22, with an average of 4.03 (Figure 3C), reinforcing the interpretation that the water conditions were saltwater during the Cambrian Niutitang deposition.

4.3 Paleoredox conditions

The assessment of paleoredox conditions in sedimentary environments is crucial for understanding the preservation potential of OM and the historical oxygenation state of the water column.

Trace elements such as vanadium (V), chromium (Cr), nickel (Ni), cobalt (Co), and uranium (U) serve as vital indicators of these conditions (Jones and Manning, 1994; Lin et al., 2008). Specifically, the concentrations of V and Ni in organic-rich sediments are highly sensitive to the prevailing redox conditions, providing insights into the oxygenation levels in various sedimentary settings (López et al., 1995; Mongenot et al., 1996). The ratio of $V/(V + Ni)$ is particularly informative: values above 0.84 are indicative of euxinic conditions, ratios between 0.54 and 0.82 suggest anoxic environments, and those ranging from 0.46 to 0.60 point to dysoxic conditions (Hatch and Leventhal, 1992; López et al., 1995; Wang X. F. et al., 2020).

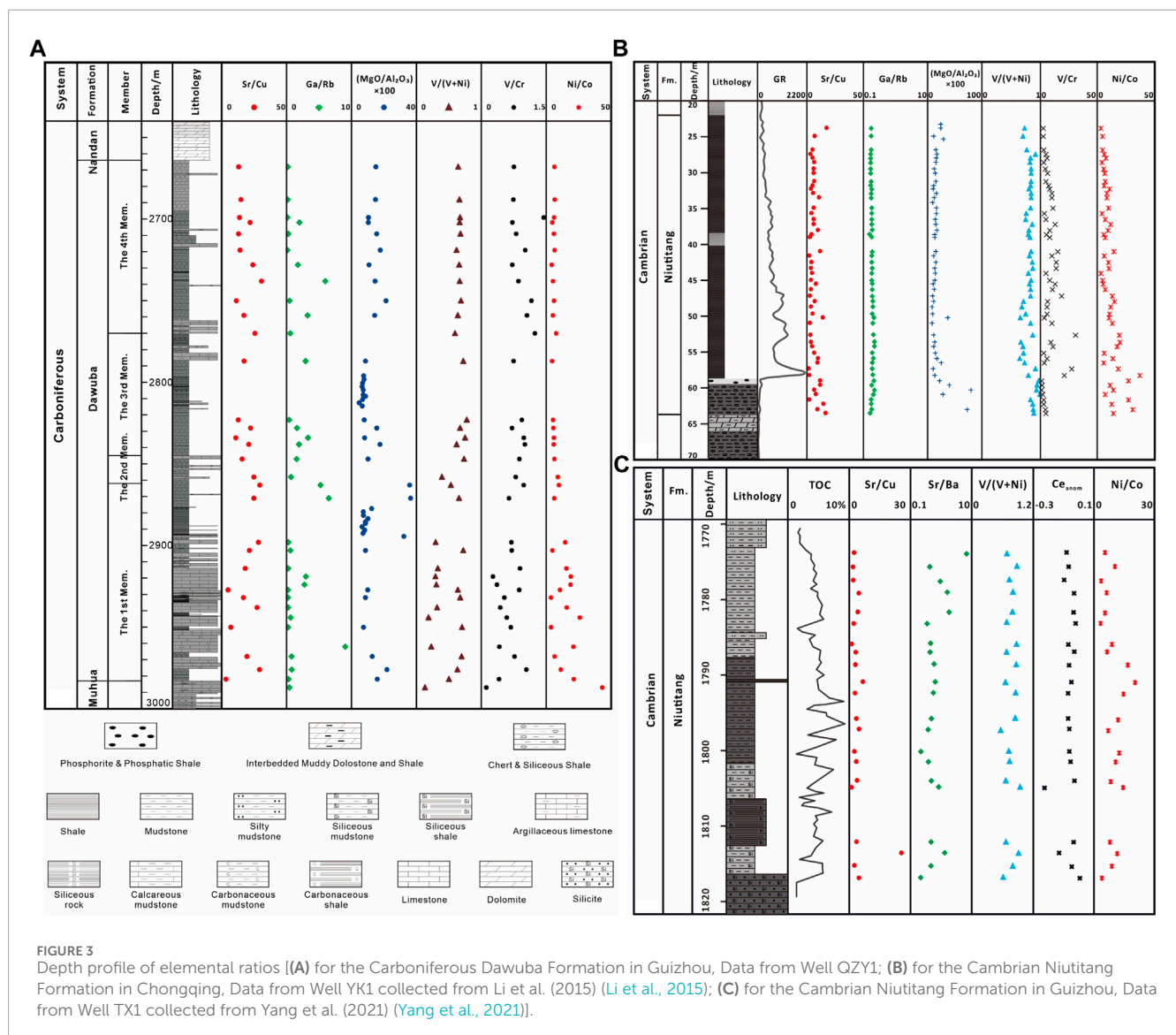
It is important to note that the enrichment of certain trace elements, such as Cr and Co, which are associated with detrital components, is less influenced by the redox state of the environment (Ross and Bustin, 2006). Thus, elevated V/Cr and Ni/Co ratios are indicative of relatively anoxic conditions. Conventionally, V/Cr ratios below two signal oxic environments, those between two and 4.25 imply dysoxic conditions, and values above 4.25 suggest anoxic conditions (Jones and Manning, 1994). Similarly, Ni/Co ratios below five denote oxic conditions, those between five and seven indicate dysoxic environments, and ratios above seven point to anoxic conditions (Jones and Manning, 1994). According to these criteria, the Dawuba shale in Guizhou, as depicted in Figure 3A, is characterized by reducing conditions, which are conducive to the preservation of OM during deposition.

According to the data collected from Li et al. (2015) (Li et al., 2015), in the Niutitang shales of the Chongqing area, V/Cr ratios range from 1.22 to 30.77, with an average of 7.94, and Ni/Co ratios vary from 2.71 to 36.80, with an average of 10.60 (Figure 3B). Additionally, the $V/(V+Ni)$ ratios range from 0.64 to 0.98, with an average of 0.80 (Figure 3B). These figures collectively indicate that the Niutitang shales were deposited under reducing conditions.

Similarly, according to the data collected from Yang et al. (2021) (Yang et al., 2021), for the Niutitang shales in the Guizhou area, $V/(V+Ni)$ ratios range from 0.58 to 0.95, with an average of 0.76, and Ni/Co ratios span from 3.38 to 20.92, with an average of 9.67 (Figure 3C). The rare earth element (REE) index Ceanom is another proxy for redox conditions, where values exceeding -0.1 suggest cerium enrichment, a positive anomaly, and thus a reducing environment (Wright et al., 1987; Zhang et al., 2017). The Ceanom values for these shales range from -0.225 to 0.006 , with an average of -0.062 (Figure 3C), further supporting the inference of reducing conditions during the Niutitang deposition in Guizhou.

4.4 Impacts of paleoenvironments on source rocks and reservoir characteristics

As demonstrated in the cases of the Niutitang and Dawuba shales, the prevailing paleoenvironments during their deposition significantly influenced their sedimentary characteristics. In both the Chongqing and Guizhou areas, the Niutitang shale was deposited under a cooler paleoclimate, saltwater conditions, and reducing environments, consistent with a deep muddy shelf in the Early Cambrian period in the Upper Yangtze region. These conditions are corroborated by previous studies (Steiner et al., 2001). In contrast, the Dawuba shale in the Guizhou area was deposited



under a warm and arid paleoclimate with transitional to marine conditions, also under reducing conditions. This aligns with the sedimentary characteristics of slope-basin facies in the Early Carboniferous period in the Upper Yangtze region, as supported by other studies (Guizhou Geological Survey Institute, 2017).

Both the Carboniferous Dawuba and Cambrian Niutitang shales experienced predominantly reducing water conditions, crucial for the preservation of organic matter (OM). Reducing environments, characterized by low oxygen levels, inhibit OM degradation by aerobic bacteria, thus enhancing its preservation. The warm and arid conditions during the Dawuba shale deposition, coupled with reducing conditions, facilitated the accumulation and preservation of OM. Conversely, the cooler and arid conditions during the Niutitang shale deposition, along with the reducing conditions, supported OM preservation. Additionally, varying paleosalinity levels influenced the type and quantity of organic matter preserved. For instance, the Dawuba shale saw a transition from transitional to predominantly saline water environments, indicating a shift towards more marine conditions

conductive to OM preservation due to factors like higher primary productivity and reduced clastic dilution. On the other hand, the Niutitang shale was deposited under stable saltwater conditions, promoting a consistent marine environment favorable for OM preservation.

Furthermore, the distinct paleoclimatic conditions under which the Dawuba and Niutitang shales were deposited significantly influenced their mineralogical compositions, impacting reservoir characteristics such as brittleness—a key feature for hydraulic fracturing. The paleoclimate affected the type and deposition of minerals, with warmer, arid conditions leading to more clay deposition and cooler, arid conditions favoring the deposition of brittle minerals like quartz and carbonates. Paleosalinity also influenced the chemical precipitation and types of minerals deposited. Meanwhile, paleoredox conditions impacted the preservation of organic matter, which indirectly influences the type and paleoproductivity of organic matter and its interplay with the mineral matrix within the shale. The warm, arid climate with transitional to saline water conditions during the Dawuba

shale deposition resulted in a mineralogy richer in clay, which typically confers ductility rather than brittleness. Conversely, the cooler, arid climate with stable saltwater conditions during the Niutitang shale deposition led to a mineralogy richer in brittle minerals, reflecting variations in chemical precipitation and sediment supply controlled by the paleoclimate and paleosalinity.

5 Evaluation of the shale source rocks

5.1 Thermal maturity

The thermal maturity of OM in sedimentary rocks is a critical factor in hydrocarbon generation, reflecting the extent of physical and chemical transformations under the influence of heat, pressure, microbial activity, subsidence, and time post-deposition (Ma et al., 2019). Parameters such as vitrinite reflectance (Ro%) and maximum pyrolysis peak temperature (Tmax) serve as reliable indicators of the thermal maturity of source rocks (Tissot and Welte, 1984; Bordenave et al., 1993).

In the Dawuba shales of Guizhou area, Ro% values range from 2.85% to 3.46%, with an average of 3.14%, as presented in Table 3 and illustrated in Figure 4, collectively suggesting that the Dawuba shales have attained a post-mature stage of thermal maturity.

For the Niutitang shales, according to the data collected from Wang (2020) (Wang, 2020) and Ge et al. (2020) (Ge et al., 2020), thermal maturity differs between locations. In the Chongqing area, Ro values span from 1.55% to 3.56%, with an average of 2.68%, whereas in the Guizhou area, they range from 1.43% to 2.81%, averaging at 2.37%. These findings indicate that the Niutitang shales in both areas have also reached the post-mature stage, suggesting significant hydrocarbon generation potential.

5.2 Organic matter abundance

The TOC content is a primary measure of OM abundance in shale source rocks. For the Dawuba shales in Guizhou, TOC values predominantly range from 0.63 to 4.25 wt%, with an average of 1.78 wt% (Table 4). According to the source rock evaluation criteria by Peters and Cassa (1994) and Tissot and Welte (1984) (Tissot and Welte, 1984; Peters et al., 1994), these values classify the Dawuba shales in Guizhou as having fair to excellent source rock potential.

According to the data collected from Wang (2020) (Wang, 2020) and Ge et al. (2020) (Ge et al., 2020), the Niutitang shales in the Chongqing area display TOC values between 0.16 wt% and 9.62 wt%, averaging at 3.43 wt%. Similarly, in the Guizhou area, TOC values range from 0.60 wt% to 8.89 wt%, with an average of 3.55 wt%. These ranges suggest that the Niutitang shales possess predominantly good to excellent source rock potential, aligning with the criteria for evaluating source rocks.

TABLE 5 (Continued) Relative content of the macerals of organic matters of the Dawuba shales in Guizhou, SW China (Data from Well QZY1).

NO.	Depth/m	Lithology	Sap. (%)			Exinite (%)				Vitrinite (%)	Inertinite (%)		TI	Type	
			Tel	Lam	Total	Cut	Sub	Res	Spo		Lipt	Total			Fusinite
ZY1-YX-247	2976	Shale	0	16	16	0	0	0	0	74	74	8	2	37	II ₂
ZY1-13-1	2981.9	Shale	0	8	8	0	0	4	0	59	63	22	7	12	II ₂
ZY1-YX-270	3010	Shale	0	28	28	0	0	4	0	54	58	11	3	31.8	II ₂

Abbreviations: Sap, sapropelinite; Tel, telalginite; Lam, lamalginite; Cut, cutinite; Sub, suberinite; Res, resinite; Spo, sporinite; Lipt, liptodetrinite. TI, $(100 \times \text{sapropelinite} + 50 \times \text{exinite} - 50 \times \text{vitrinite} - 75 \times \text{inertinite}) / 100$.

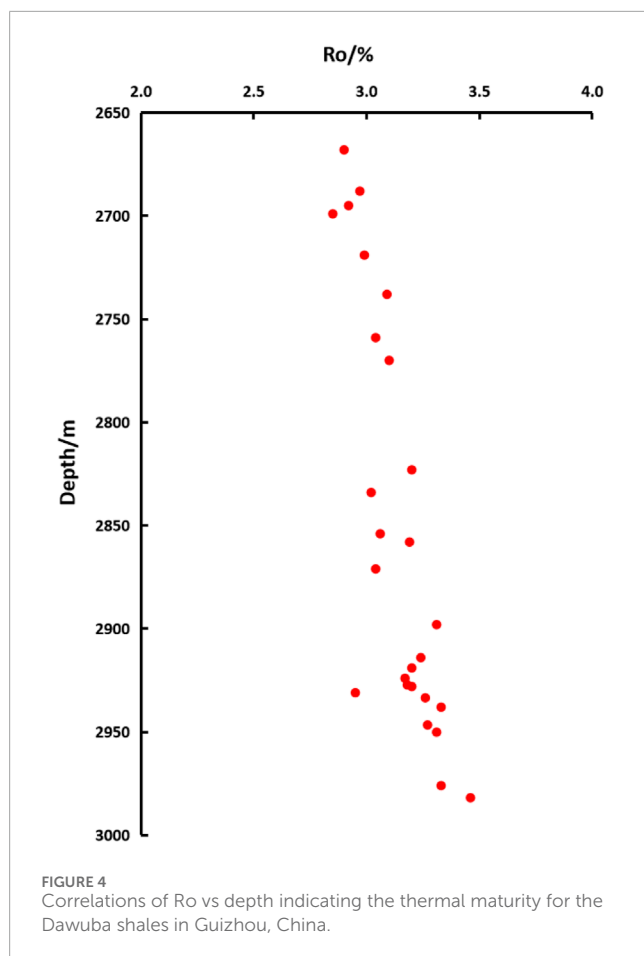
TABLE 3 Vitrinite reflectance (R_o %) data of the Dawuba shales in Guizhou, SW China (Data from Well QZY1).

No.	Depth/m	Min	Max	Avg	Standard deviation	Points
ZY1-YX-1	2668.00	—	—	2.90	—	1
ZY1-YX-3	2688.00	2.80	3.13	2.97	0.15	3
ZY1-4-01	2695.00	2.75	3.11	2.92	0.16	5
ZY1-4-05	2699.00	2.66	3.02	2.85	0.18	4
ZY1-YX-85	2719.00	2.86	3.13	2.99	0.15	3
ZY1-YX-9	2738.00	2.92	3.22	3.09	0.14	4
ZY1-YX-119	2759.00	2.88	3.25	3.04	0.18	3
ZY1-YX-16	2770.00	2.97	3.27	3.10	0.15	3
ZY1-YX-151	2823.00	3.03	3.39	3.20	0.13	3
ZY1-YX-160	2834.00	2.88	3.21	3.02	0.18	3
ZY1-YX-178	2854.00	2.90	3.22	3.06	0.12	4
ZY1-YX-28	2858.00	3.03	3.35	3.19	0.13	4
ZY1-YX-193	2871.00	2.87	3.27	3.04	0.16	4
ZY1-YX-32	2898.00	3.14	3.52	3.31	0.16	4
ZY1-YX-33	2914.00	3.05	3.47	3.24	0.16	5
ZY1-YX-220	2919.00	3.03	3.42	3.2	0.17	4
ZY1-YX-225	2924.00	3.00	3.45	3.17	0.16	5
ZY1-10-2	2927.20	—	—	3.18	—	1
ZY1-10-3	2928.00	—	—	3.20	—	1
ZY1-10-6	2931.00	2.77	3.12	2.95	0.17	4
10-1	2933.48	3.07	3.42	3.26	0.18	5
ZY1-YX-36	2938.00	—	—	3.33	—	1
ZY1-12-2	2946.60	3.09	3.50	3.27	0.16	4
ZY1-12-5	2950.10	3.14	3.48	3.31	0.14	3
ZY1-YX-247	2976.00	3.16	3.55	3.33	0.17	4
ZY1-13-1	2981.90	3.28	3.66	3.46	—	4

5.3 Organic matter types

Given that the type of OM significantly influences the properties, composition, and quantity of hydrocarbon generation (Peters et al., 1994), identifying the kerogen type within potential source rocks is crucial. The maceral compositions, namely, liptinite, vitrinite, and inertinite, serve as the basis for this classification. In the context of China, liptinite is further categorized into sapropelinite and exinite, with sapropelinite encompassing lginate

and sapropelic amorphous material, and exinite including various forms like cutinite, suberinite, sporinite, resinite, exsudatinitite, chlorophyllinitite, liptodetrinitite, and bituminite. The proportions of liptinite, vitrinite, and inertinite within the Dawuba shales in Guizhou are detailed in Table 5. Specifically, in the shales, liptinites, which are primarily composed of liptodetrinitite, exhibit a range between 71% and 92%, with an average of 82.6%. Vitrinite, characterized by its distinct outlines, varies from 5% to 22%, averaging at 13.3%, as depicted in Figure 5. Inertinite,



mainly consisting of fusinite, ranges from 1% to 8%, with an average of 4.1%.

The kerogen type is ascertainable through the TI index, as defined by Mukhopadhyay et al. (1995) (Mukhopadhyay et al., 1995) and Hakimi et al. (2011) (Hakimi et al., 2011): $(TI = (100 \times \text{sapropelite} + 50 \times \text{exinite} - 50 \times \text{vitrinite} - 75 \times \text{inertinite})/100)$. TI indexes are interpreted as follows: greater than 80 for Type I, between 80 and 40 for Type II1, between 40 and 0 for Type II2, and less than 0 for Type III kerogens.

The Dawuba shales in Guizhou predominantly exhibit TI indexes ranging from 0 to 40, indicative of Type II2 kerogens, as summarized in Table 5. Studies by Wang (2020) (Wang, 2020) and Ge et al. (2020) (Ge et al., 2020) suggest that the kerogen types in the Niutitang shales, specifically within the Chongqing and Guizhou areas, are predominantly Type I, with some instances of Type II1. This conclusion is supported by the observed maceral compositions (Ge et al., 2020; Wang, 2020).

Consequently, the source rocks of the Niutitang shales in both the Chongqing and Guizhou areas are characterized as post-mature, with predominantly good to excellent generation potential, and primarily contain Type I kerogens. Concurrently, the source rocks of the Dawuba shales in the Guizhou area are also post-mature but exhibit a range of fair to excellent generation potential, and contain Type II2 kerogens. These characteristics indicate that both the Niutitang and Dawuba shales possess significant gas generation potential.

TABLE 4 TOC data of the Dawuba shale in Guizhou, SW China (Data from Well QZY1).

No.	Depth/m	Lithology	TOC (wt%)
ZY1-YX-1	2668	Shale	1.02
ZY1-YX-2	2678	Shale	1.02
ZY1-YX-3	2688	Shale	0.95
ZY1-4-01	2695	Shale	0.63
ZY1-4-05	2699	Shale	0.94
ZY1-YX-76	2709	Shale	0.88
ZY1-YX-85	2719	Shale	0.79
ZY1-YX-8	2728	Shale	1.40
ZY1-YX-9	2738	Shale	1.39
ZY1-YX-11	2750	Shale	0.78
ZY1-YX-119	2759	Shale	1.12
ZY1-YX-136	2787	Shale	2.05
ZY1-6-01	2796	Shale	3.90
ZY1-6-06	2801.4	Shale	4.25
ZY1-6-08	2803.6	Shale	2.99
ZY1-7-06	2810.5	Shale	2.01
ZY1-YX-151	2823	Shale	2.44
ZY1-YX-25	2828	Shale	0.97
ZY1-YX-26	2838	Shale	1.04
ZY1-YX-172	2847	Shale	2.30
ZY1-YX-193	2871	Shale	1.33
ZY1-8-03	2878.4	Shale	1.56
ZY1-8-04	2879.4	Shale	1.52
ZY1-8-10	2885.5	Shale	1.34
ZY1-9-02	2886.5	Shale	1.27
ZY1-9-07	2891.5	Shale	1.52
ZY1-9-08	2892.5	Shale	1.48
ZY1-10-2	2927.2	Shale	3.75
ZY1-10-7	2931.95	Shale	1.91
10-1	2933.48	Shale	2.17
ZY1-12-5	2950.1	Shale	2.48
ZY1-YX-247	2976	Shale	2.25
ZY1-13-1	2981.9	Shale	3.38

TABLE 5 Relative content of the macerals of organic matters of the Dawuba shales in Guizhou, SW China (Data from Well QZ Y1).

NO.	Depth/m	Lithology	Sap. (%)			Exinite (%)					Vitrinite (%)	Inertinite (%)		TI	Type
			Tel	Lam	Total	Cut	Sub	Res	Spo	Lipt		Total	Fusinite		
ZY1-YX-1	2668	Shale	0	13	13	0	0	2	0	0	67	69	4	26.5	II ₂
ZY1-YX-3	2688	Shale	0	18	18	0	0	4	0	0	56	60	5	21.3	II ₂
ZY1-YX-5	2702	Shale	0	20	20	0	0	2	0	0	63	65	2	30.8	II ₂
ZY1-YX-85	2719	Shale	0	28	28	0	0	0	0	0	59	59	3	33	II ₂
ZY1-YX-9	2738	Shale	0	17	17	0	0	0	0	0	64	64	3	25.5	II ₂
ZY1-YX-11	2750	Shale	0	22	22	0	0	0	0	0	63	63	3	30.5	II ₂
ZY1-YX-119	2759	Shale	0	17	17	0	0	3	0	0	56	59	8	18	II ₂
ZY1-6-01	2796	Shale	0	12	12	0	0	0	0	0	74	74	1	32.3	II ₂
ZY1-6-07	2802.6	Shale	0	11	11	0	0	0	0	0	73	73	2	29.5	II ₂
ZY1-7-02	2806.5	Shale	0	13	13	0	0	0	0	0	72	72	4	30.3	II ₂
ZY1-7-08	2812.5	Shale	0	15	15	0	0	0	0	0	64	64	5	22.5	II ₂
ZY1-YX-151	2823	Shale	0	26	26	0	0	0	0	0	58	58	5	28.8	II ₂
ZY1-YX-26	2838	Shale	0	24	24	0	0	5	0	0	47	52	6	18.5	II ₂
ZY1-YX-193	2871	Shale	0	20	20	0	0	0	0	0	65	65	3	30.5	II ₂
ZY1-8-02	2877.4	Shale	0	19	19	0	0	0	0	0	63	63	4	26.5	II ₂
ZY1-8-07	2882.5	Shale	0	16	16	0	0	0	0	0	76	76	3	39.3	II ₂
ZY1-8-10	2885.5	Shale	0	12	12	0	0	0	0	0	75	75	2	33.3	II ₂
ZY1-9-02	2886.5	Shale	0	12	12	0	0	0	0	0	80	80	2	39.5	II ₂
ZY1-9-06	2890.5	Shale	0	16	16	0	0	0	0	0	69	69	4	30.3	II ₂
ZY1-10-7	2931.95	Shale	0	14	14	0	0	5	0	0	61	66	5	23.8	II ₂
10-1	2933.48	Shale	0	14	14	0	0	4	0	0	57	61	8	16.8	II ₂
11-1	2942.75	Shale	0	22	22	0	0	0	0	0	62	62	4	29	II ₂

(Continued on the following page)

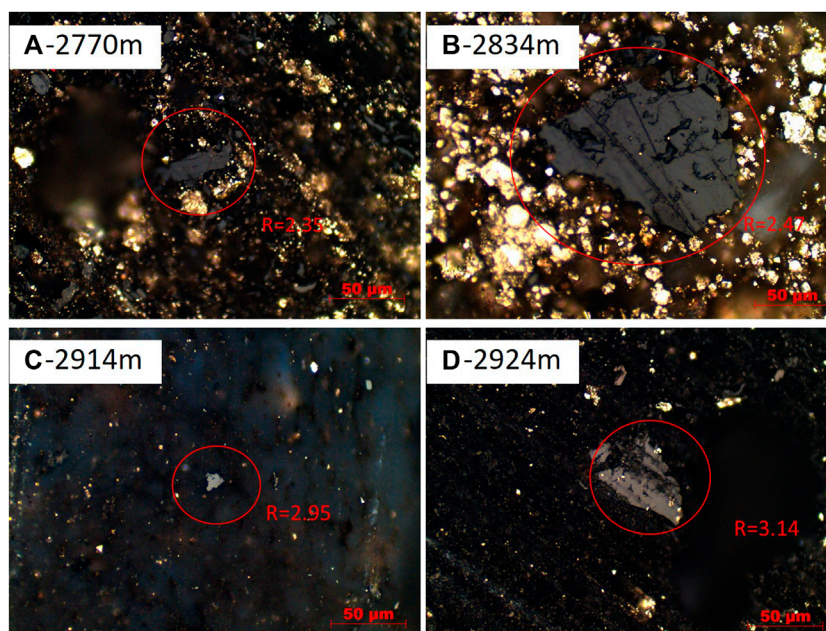


FIGURE 5

Photomicrographs of identified vitrinite in the Dawuba shales in Guizhou area under oil-immersed reflected light. (A) for sample depth of 2770 m, (B) for sample depth of 2834 m, (C) for sample depth of 2914 m, and (D) for sample depth of 2924 m.

6 Shale reservoir characteristics

6.1 Mineralogy characteristics

The mineralogical composition of the Dawuba shales in Guizhou is characterized by a significant presence of clay minerals, ranging from 4.0% to 62.0%, with an average of 44.3%, and quartz, ranging from 15.0% to 68.0%, with an average of 33.2%. Other constituents include carbonates (0%–54.0%, Avg.=15.7%), pyrite (0%–13.0%, Avg.=4.75%), and feldspar (0%–11.0%, Avg.=2.02%) (Figure 6A; Table 6). The clay minerals are predominantly illite (Avg.=74.7%), followed by mixed-layer illite-smectite (I/S, Avg.=16.3%) and chlorite (Avg.=7.4%) (Figure 6B; Table 6). This composition suggests that, compared to the Chang-7 lacustrine shale in the Ordos Basin and the Longmaxi marine shale in South China, the Dawuba shales in Guizhou have a lower content of brittle minerals (such as quartz, feldspar, and carbonates) and a higher proportion of clays.

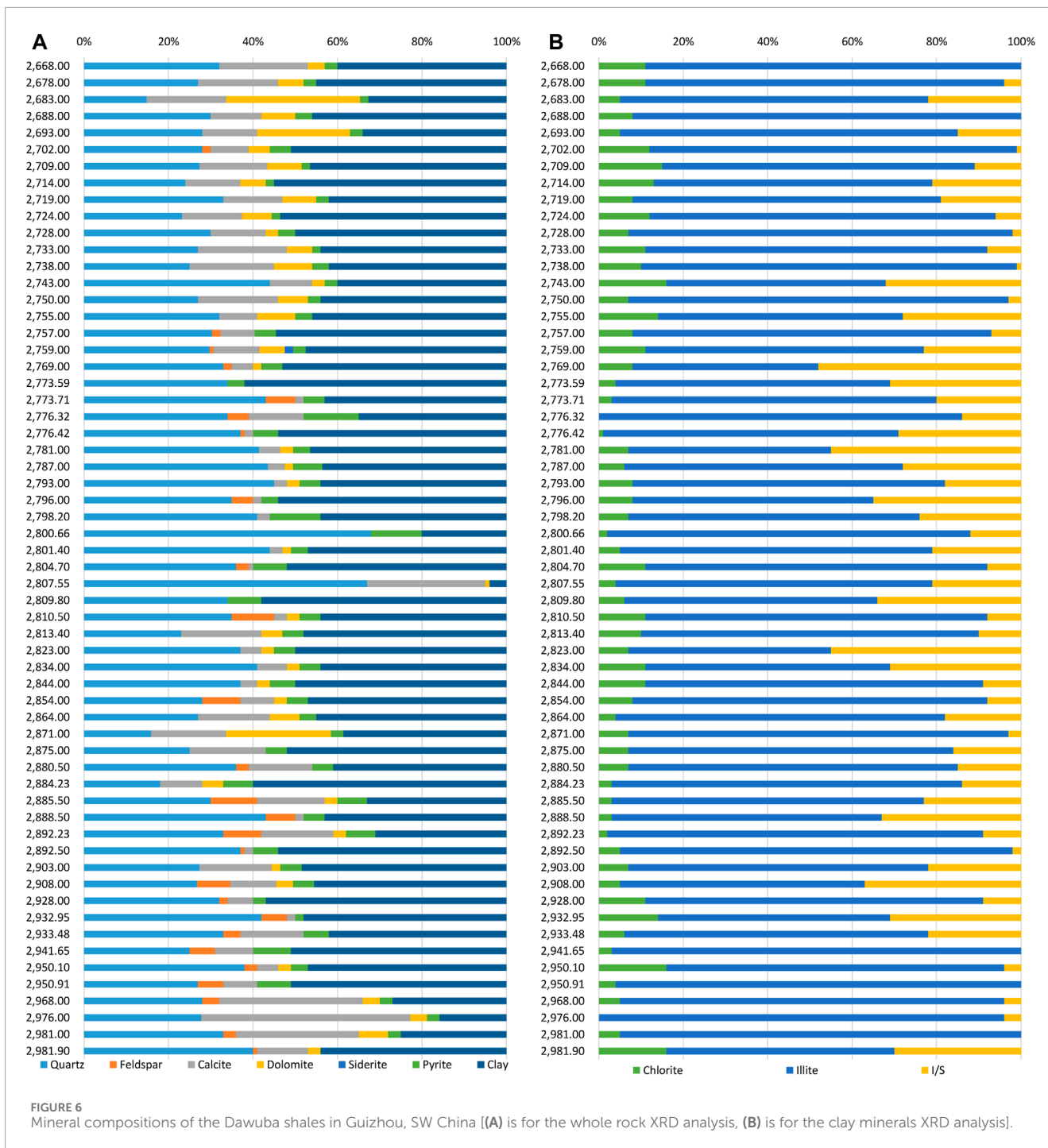
According to the data collected from Ge et al. (2020) (Ge et al., 2020), the Niutitang shales in the Guizhou area display a relatively high content of brittle minerals, with overall ranges from 37% to 68%, and an average of 51%. Quartz content varies from 28.0% to 53.0%, averaging 37.8%, while clay mineral content ranges from 18.0% to 58.0%, with an average of 38.3% (Figure 7A). Carbonate minerals are also present, albeit with few pyrites. The dominant clay mineral is the I/S mixed layer, which ranges from 47.0% to 64.0%, averaging 56.1% (Figure 7B), indicating strong adsorption capacity in the Niutitang Formation shale of Well HD1. Illite and a small amount of chlorite are also present, with montmorillonite absent, suggesting its complete conversion to illite under high-to over-mature conditions.

Shale classification into calcareous, siliceous, argillaceous, and mixed types is based on the relative contents of calcareous,

siliceous, and argillaceous minerals, with a classification threshold set at greater than 50% (Dong et al., 2016). In the Guizhou area, both the Dawuba and Niutitang shales exhibit similar classifications. Specifically, the Dawuba shales, which are richer in clay minerals, are predominantly classified as argillaceous (31.7%) and mixed (61.7%). Conversely, the Niutitang shales, which contain higher amounts of brittle minerals, are primarily mixed shale (66.7%) and argillaceous shale (26.7%). These compositional differences have significant implications for shale gas exploration. The Niutitang shales, being rich in brittle minerals, tend to preserve more solid hosted (meso and macro) porosity compared to the more clay-rich Dawuba shales of similar maturity. This characteristic makes the Niutitang shales more amenable to hydraulic fracturing, a key technique used in shale gas extraction, due to the presence of more brittle minerals which facilitate the fracturing process.

6.2 Physical properties

The physical properties of shale, specifically porosity and permeability, are critical in evaluating its potential as a hydrocarbon reservoir. For the Dawuba shale samples in Guizhou, data presented in Table 7 indicate that porosity values range from 0.88% to 5.92%, averaging 3.45%. Permeability values vary from 0.0009 to 0.0441 millidarcies (mD), with an average of 0.0098 mD (Table 7). These values suggest that the Dawuba shales generally exhibit low porosity and permeability. However, a notable exception is observed within the first member of the formation, where both porosity and permeability show relatively higher values. This improvement can be attributed to the presence of various pore types, including



inorganic and organic pores, as well as bedding fractures. These features collectively enhance the formation's potential as an effective hydrocarbon reservoir by facilitating fluid flow.

According to the study conducted by Ge et al. (2020), the Niutitang shales from Well HD-1 in the Guizhou area were characterized by their porosity and permeability values. The porosity of these shales ranged from 0.2% to 1.8%, with an average value of 0.51%. Similarly, permeability values were found to range between 0.0001 mD and 0.01 mD, with an average value of 0.001 mD. These measurements

categorize the reservoir as having ultra-low porosity and ultra-low permeability.

6.3 Pore structure characteristics

The pore structure of shale significantly influences its capacity to store and transmit hydrocarbons. In the Dawuba shales of Guizhou, pore types identified under Field Emission Scanning Electron Microscopy (FE-SEM) primarily include inter-particle

TABLE 6 XRD data of the Dawuba shale in Guizhou, SW China (Data from Well QZY1).

No.	Depth/m	Lithology	Q/%	Fr/%	CaL/%	DoL/%	SidL/%	PyL/%	Clay/%	S/%	I/%	K/%	C/%	I/S	S/%	I/%
ZY1-YX-1	2668.00	Shale	32	0	21	4	0	3	40	0	89	0	11	0	10	90
ZY1-YX-2	2678.00	Shale	27	0	19	6	0	3	45	0	85	0	11	4	10	90
ZY1-YX-60	2683.00	Shale	15	0	19	32	0	2	33	0	73	0	5	22	10	90
ZY1-YX-3	2688.00	Shale	30	0	12	8	0	4	46	0	92	0	8	0	10	90
ZY1-YX-69	2693.00	Shale	28	0	13	22	0	3	34	0	80	0	5	15	10	90
ZY1-YX-5	2702.00	Shale	28	2	9	5	0	5	51	0	87	0	12	1	5	95
ZY1-YX-76	2709.00	Shale	27	0	16	8	0	2	46	0	74	0	15	11	10	90
ZY1-YX-81	2714.00	Shale	24	0	13	6	0	2	55	0	66	0	13	21	10	90
ZY1-YX-85	2719.00	Shale	33	0	14	8	0	3	42	0	73	0	8	19	10	90
ZY1-YX-90	2724.00	Shale	23	0	14	7	0	2	53	0	82	0	12	6	10	90
ZY1-YX-8	2728.00	Shale	30	0	13	3	0	4	50	0	91	0	7	2	10	90
ZY1-YX-98	2733.00	Shale	27	0	21	6	0	2	44	0	81	0	11	8	10	90
ZY1-YX-9	2738.00	Shale	25	0	20	9	0	4	42	0	89	0	10	1	10	90
ZY1-YX-107	2743.00	Shale	44	0	10	3	0	3	40	0	52	0	16	32	10	90
ZY1-YX-11	2750.00	Shale	27	0	19	7	0	3	44	0	90	0	7	3	10	90
ZY1-YX-116	2755.00	Shale	32	0	9	9	0	4	46	0	58	0	14	28	10	90
ZY1-YX-13	2757.00	Shale	30	2	8	0	0	5	54	0	85	0	8	7	10	90
ZY1-YX-119	2759.00	Shale	30	1	11	6	2	3	48	0	66	0	11	23	10	90
ZY1-YX-127	2769.00	Shale	33	2	5	2	0	5	53	0	44	0	8	48	10	90
5-1	2773.59	Shale	34	0	0	0	0	4	62	0	65	0	4	31	15	85
ZY1-5-02	2773.71	Shale	43	7	2	0	0	5	43	0	77	0	3	20	15	85
5-3	2776.32	Shale	34	5	13	0	0	13	35	0	86	0	0	14	10	90
ZY1-5-06	2776.42	Shale	37	1	2	0	0	6	54	0	70	0	1	29	10	90

(Continued on the following page)

TABLE 6 (Continued) XRD data of the Dawuba shale in Guizhou, SW China (Data from Well QZY1).

No.	Depth/m	Lithology	Q/%	Fr/%	CaL/%	DoL/%	Sid.t./%	Pyt./%	Clay/%	S/%	I/%	K/%	C/%	I/S	S/%	I/%
ZY1-YX-130	2781.00	Shale	41	0	5	3	0	4	46	0	48	0	7	45	10	90
ZY1-YX-136	2787.00	Shale	44	0	4	2	0	7	44	0	66	0	6	28	10	90
ZY1-YX-141	2793.00	Shale	45	0	3	3	0	5	44	0	74	0	8	18	10	90
ZY1-6-01	2796.00	Shale	35	5	2	0	0	4	54	0	57	0	8	35	5	95
ZY1-6-03	2798.20	Shale	41	0	3	0	0	12	44	0	69	0	7	24	5	95
6-2	2800.66	Shale	68	0	0	0	0	12	20	0	86	0	2	12	15	85
ZY1-6-06	2801.40	Shale	44	0	3	2	0	4	47	0	74	0	5	21	5	95
ZY1-6-09	2804.70	Shale	36	3	1	0	0	8	52	0	81	0	11	8	5	95
ZY1-7-03	2807.55	Shale	67	0	28	1	0	0	4	0	75	0	4	21	5	95
7-2	2809.80	Shale	34	0	0	0	0	8	58	0	60	0	6	34	15	85
ZY1-7-06	2810.50	Shale	35	10	3	3	0	5	44	0	81	0	11	8	5	95
ZY1-7-09	2813.40	Shale	23	0	19	5	0	5	48	0	80	0	10	10	0	0
ZY1-YX-151	2823.00	Shale	37	0	5	3	0	5	50	0	48	0	7	45	10	90
ZY1-YX-160	2834.00	Shale	41	0	7	3	0	5	44	0	58	0	11	31	10	90
ZY1-YX-169	2844.00	Shale	37	0	4	3	0	6	50	0	80	0	11	9	10	90
ZY1-YX-178	2854.00	Shale	28	9	8	3	0	5	47	0	84	0	8	8	10	90
ZY1-YX-187	2864.00	Shale	27	0	17	7	0	4	45	0	78	0	4	18	10	90
ZY1-YX-193	2871.00	Shale	16	0	18	25	0	3	39	0	90	0	7	3	10	90
ZY1-YX-197	2875.00	Shale	25	0	18	0	0	5	52	0	77	0	7	16	10	90
ZY1-8-05	2880.50	Shale	36	3	15	0	0	5	41	0	78	0	7	15	10	90
8-1	2884.23	Shale	18	0	10	5	0	7	60	0	83	0	3	14	15	85
ZY1-8-10	2885.50	Shale	30	11	16	3	0	7	33	0	74	0	3	23	10	90
ZY1-9-04	2888.50	Shale	43	7	2	0	0	5	43	0	64	0	3	33	10	90

(Continued on the following page)

TABLE 6 (Continued) XRD data of the Dawuba shale in Guizhou, SW China (Data from Well QZY1).

No.	Depth/m	Lithology	Q/%	Fr/%	Cal./%	Dol./%	Sidt./%	Pyt./%	Clay/%	S/%	I/%	K/%	C/%	I/S	S/%	I/%
9-1	2892.23	Shale	33	9	17	3	0	7	31	0	89	0	2	9	15	85
ZY1-9-08	2892.50	Shale	37	1	2	0	0	6	54	0	93	0	5	2	10	90
ZY1-YX-206	2903.00	Shale	27	0	17	2	0	5	48	0	71	0	7	22	10	90
ZY1-YX-211	2908.00	Shale	27	8	11	4	0	5	46	0	58	0	5	37	10	90
ZY1-10-3	2928.00	Shale	32	2	6	0	0	3	57	0	80	0	11	9	10	90
ZY1-10-8	2932.95	Shale	42	6	2	0	0	2	48	0	55	0	14	31	10	90
10-1	2933.48	Shale	33	4	15	0	0	6	42	0	72	0	6	22	10	90
11-2	2941.65	Shale	25	6	9	0	0	9	51	0	97	0	3	0	0	0
ZY1-12-5	2950.10	Shale	38	3	5	3	0	4	47	0	80	0	16	4	10	90
12-2	2950.91	Shale	27	6	8	0	0	8	51	0	96	0	4	0	0	0
ZY1-YX-39	2968.00	Shale	28	4	34	4	0	3	27	0	91	0	5	4	10	90
ZY1-YX-247	2976.00	Shale	28	0	50	4	0	3	16	0	96	0	0	4	10	90
13-1	2981.00	Shale	33	3	29	7	0	3	25	0	95	0	5	0	0	0
ZY1-13-1	2981.90	Shale	40	1	12	3	0	0	44	0	54	0	16	30	10	90

Abbreviations: Q, Quartz; F, Feldspar; Ca, calcite; Dol, dolomite; Sidt, siderite; Pyt, pyrite; Clay, Clay minerals; S, smectite; I, illite; K, kaolinite; C, chlorite; I/S, mixed layer of illite and smectite.

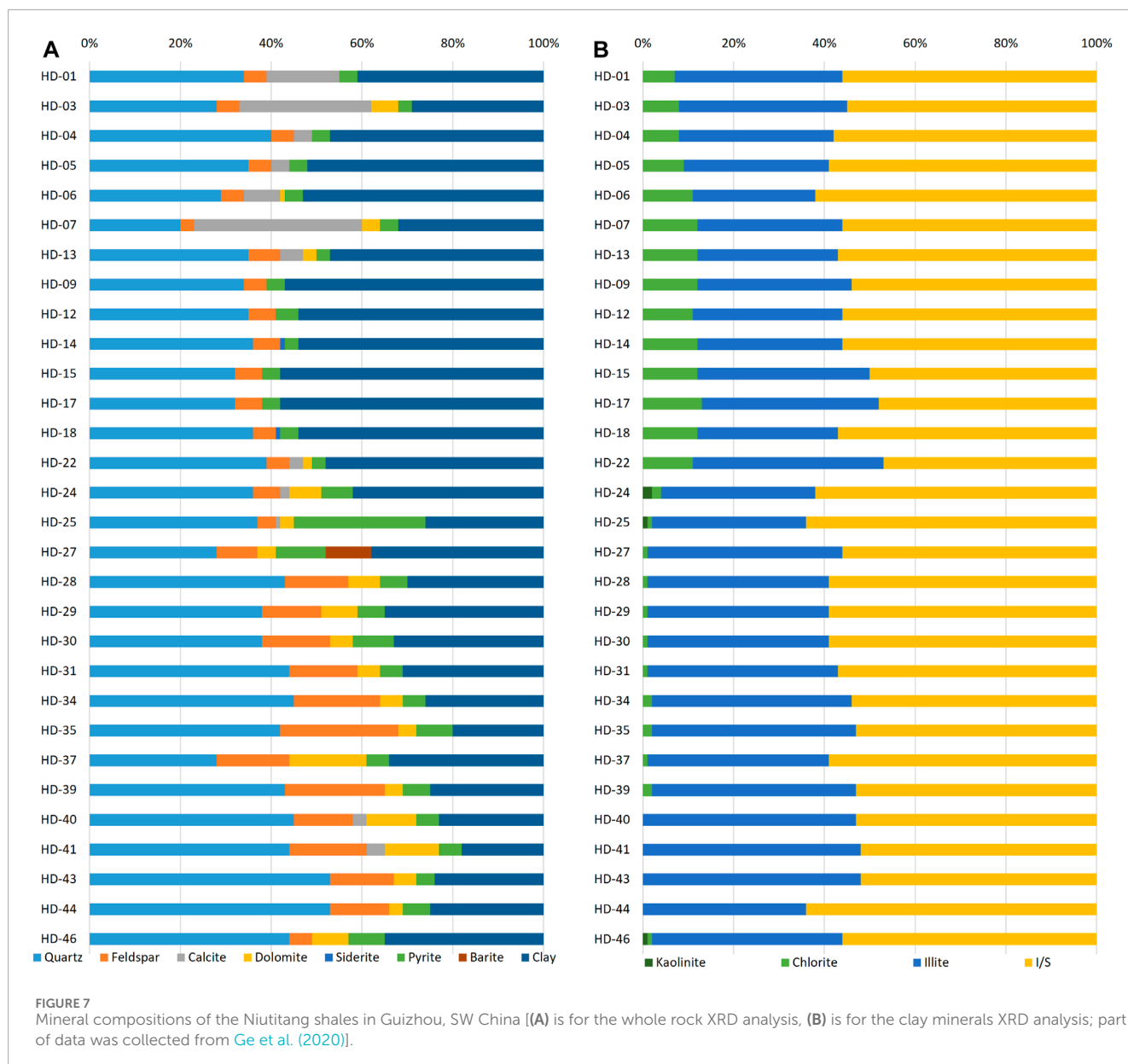


TABLE 7 Porosity and permeability of the Dawuba shale in Guizhou, SW China.

No.	Depth/m	Lithology	Porosity/%	Permeability/mD
8-1	2884.23	Shale	4.88	0.0441
9-2	2891.00	Shale	5.92	0.0037
11-1	2942.75	Shale	4.27	0.0056
ZY1-11-7	2943.07	Shale	1.59	0.0017
ZY1-12-6	2945.42	Shale	3.15	0.0009
13-1	2981.00	Shale	0.88	0.0028

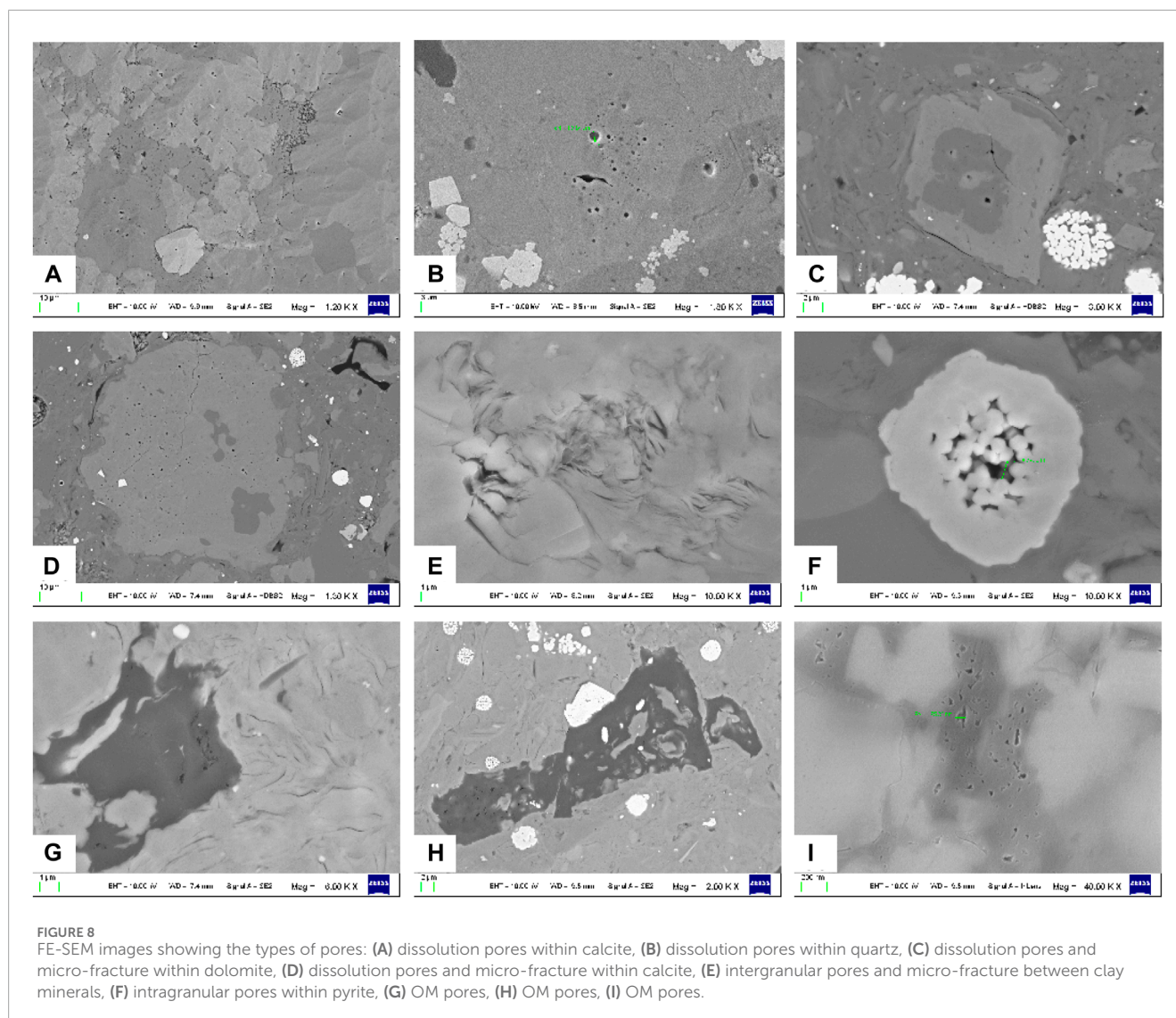


FIGURE 8
FE-SEM images showing the types of pores: (A) dissolution pores within calcite, (B) dissolution pores within quartz, (C) dissolution pores and micro-fracture within dolomite, (D) dissolution pores and micro-fracture within calcite, (E) intergranular pores and micro-fracture between clay minerals, (F) intragranular pores within pyrite, (G) OM pores, (H) OM pores, (I) OM pores.

pores (Inter-P), intra-particle pores (Intra-P), and OM pores, as illustrated in Figure 8. Intra-P pores are mainly inter-crystalline within pyrite and clay minerals and dissolution pores within calcite and quartz or along particle rims. Inter-P pores, situated between mineral grains, are polygonal, elongated, or slit-like and exhibit good connectivity. OM pores are predominantly spongy, with bubble-like OM pores being uniformly and independently distributed within the OM.

According to a study by Ge et al. (2024), the Niutitang shales in the Guizhou area feature micro-storage spaces dominated by matrix pores and fractures, including diagenetic fractures, layered clay mineral interlayer pores, and pyrite intercrystalline pores. Additionally, interstitial organic pores are present, featuring a size range of 10–150 nm. The pyrite observed is often in the form of strawberry-shaped or aggregate shapes, frequently coexisting with OM. Furthermore, a minor presence of residual pores and intragranular pores has also been noted (Ma et al., 2015).

Isothermal adsorption curves, which often form a hysteresis loop separating from the desorption curve within a specific pressure range, are influenced by the relative pressure of capillary

condensation and evaporation, varying with pore morphology. By analyzing the shapes of hysteresis loops, it is possible to speculate about the morphology of the pore shape (Sing, 1995). In this study, the shapes of the N₂ adsorption and desorption isotherms displayed minimal differences, as shown in Figures 9, 10.

N₂ adsorption was employed to quantify the mesopore and macropore structures in both Dawuba and Niutitang shales in Guizhou. The N₂ adsorption-desorption isotherms showed similar trends across all shale samples, indicating a broad adsorption range. The volumes of adsorption at $P/P_0 < 0.05$ and near $P/P_0 = 1.0$ suggest the presence of microporosity and macroporosity, respectively (Clarkson et al., 2013). As P/P_0 increases to 0.5, a hysteresis loop appears between the adsorption and desorption branches, indicating the presence of mesopores (Kuila and Prasad, 2013). According to the IUPAC, the N₂ adsorption isotherms follow the Type IV classification, and the hysteresis loops exhibit an intermediate type between types H2 and H3, with hysteresis loops suggesting inkbottle and slit pore shapes, although SEM analyses confirm the polymorphic nature of shale pore shapes.

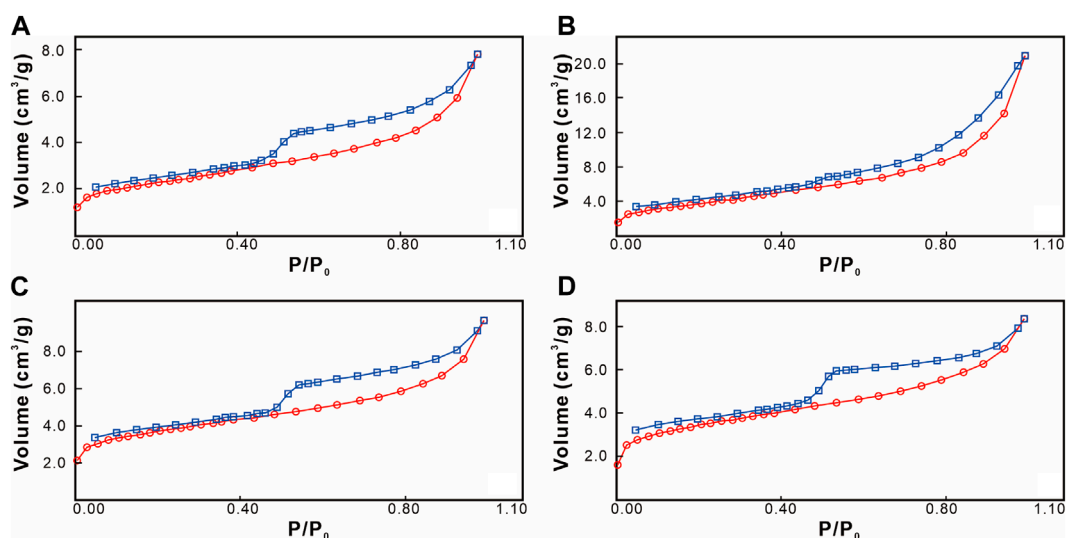


FIGURE 9 N2 isotherms of the Dawuba shale in Guizhou, SW China (Data from Well QZY1; (A) for the sample depth of 2708 m, (B) for the sample depth of 2828 m, (C) for the sample depth of 2883.7 m, (D) for the sample depth of 2951.75 m).

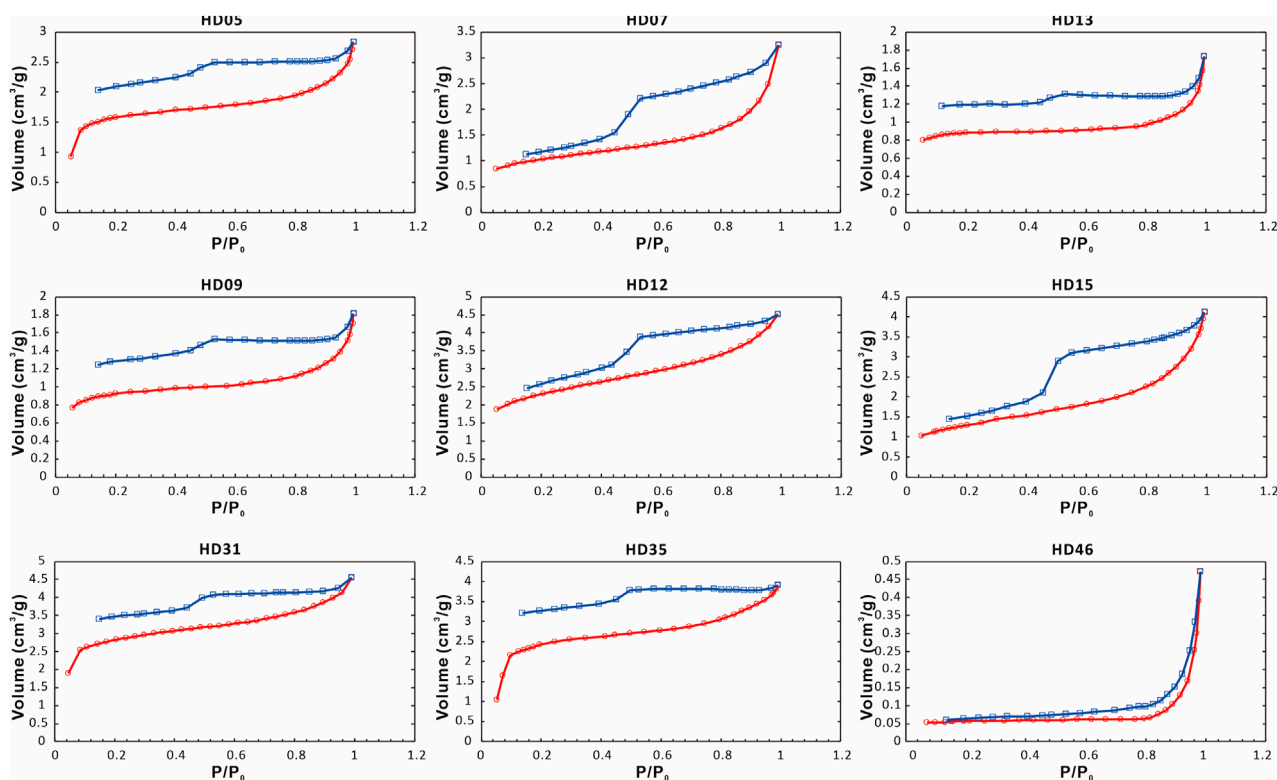


FIGURE 10 N2 isotherms of the Niutitang shale in Guizhou, SW China (Data from Well HD1).

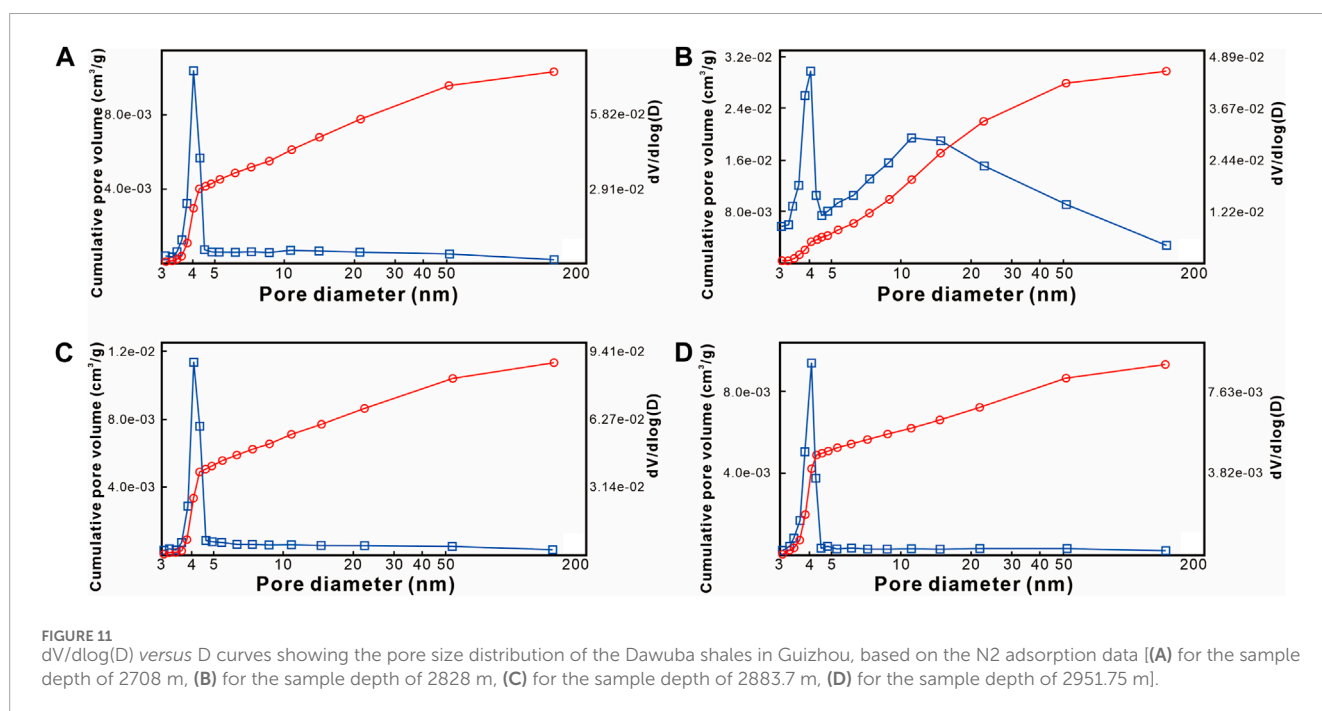
Accurate characterization of the nanoscale pore system in shales requires the selection of appropriate methods for determining low-pressure gas adsorption. In this study, the DFT model was used to calculate the specific surface area (SSA) and pore volume (PV) of micropores, while the NLDFT model was applied to determine

the SSA and PV of mesopores and macropores, based on the applicable conditions and principles of these methods (Sing, 1995; Clarkson et al., 2013; Kuila and Prasad, 2013).

As detailed in Table 8, the Dawuba shales in Guizhou exhibited BET-specific surface areas ranging from 8.126 to 13.937 m²/g,

TABLE 8 Porosity and permeability of the Dawuba shale in Guizhou, SW China.

Layer	Sample no.	BET surface areas (m ² /g)	BJH total pore volumes (x10 ⁻³ cm ³ /g)	Average pore diameters(nm)
Dawuba	QZY1-1	8.126	5.924	5.924
	QZY1-2	13.937	9.267	9.267
	QZY1-3	13.329	4.487	4.487
	QZY1-4	12.280	4.194	4.194
Niutitang	HD05	5.670	2.090	3.09
	HD07	3.532	4.130	5.69
	HD13	2.835	1.020	3.77
	HD09	3.063	1.340	3.66
	HD12	7.874	4.240	3.54
	HD15	4.484	6.520	5.69
	HD31	4.782	1.720	2.75
	HD35	9.800	2.010	2.46
	HD46	0.178	0.634	16.81



with an average of 11.918 m²/g. The total pore volumes ranged from 12.03x10⁻³ to 32.29x10⁻³ cm³/g, averaging 18.03x10⁻³ cm³/g. The average pore diameters varied from 4.194 to 9.267 nm, with a mean of 5.968 nm. The pore size distribution (PSD), plotted as dV/dlog(D) versus D curves using the BJH model on the adsorption branches, showed one sample with a bimodal

curve and three samples with unimodal curves, indicating a predominance of micropores and mesopores, as depicted in Figure 11.

Conversely, the Niutitang shales in Guizhou showed BET-specific surface areas ranging from 0.178 to 7.874 m²/g, with an average of 4.691 m²/g. The total pore volumes varied from

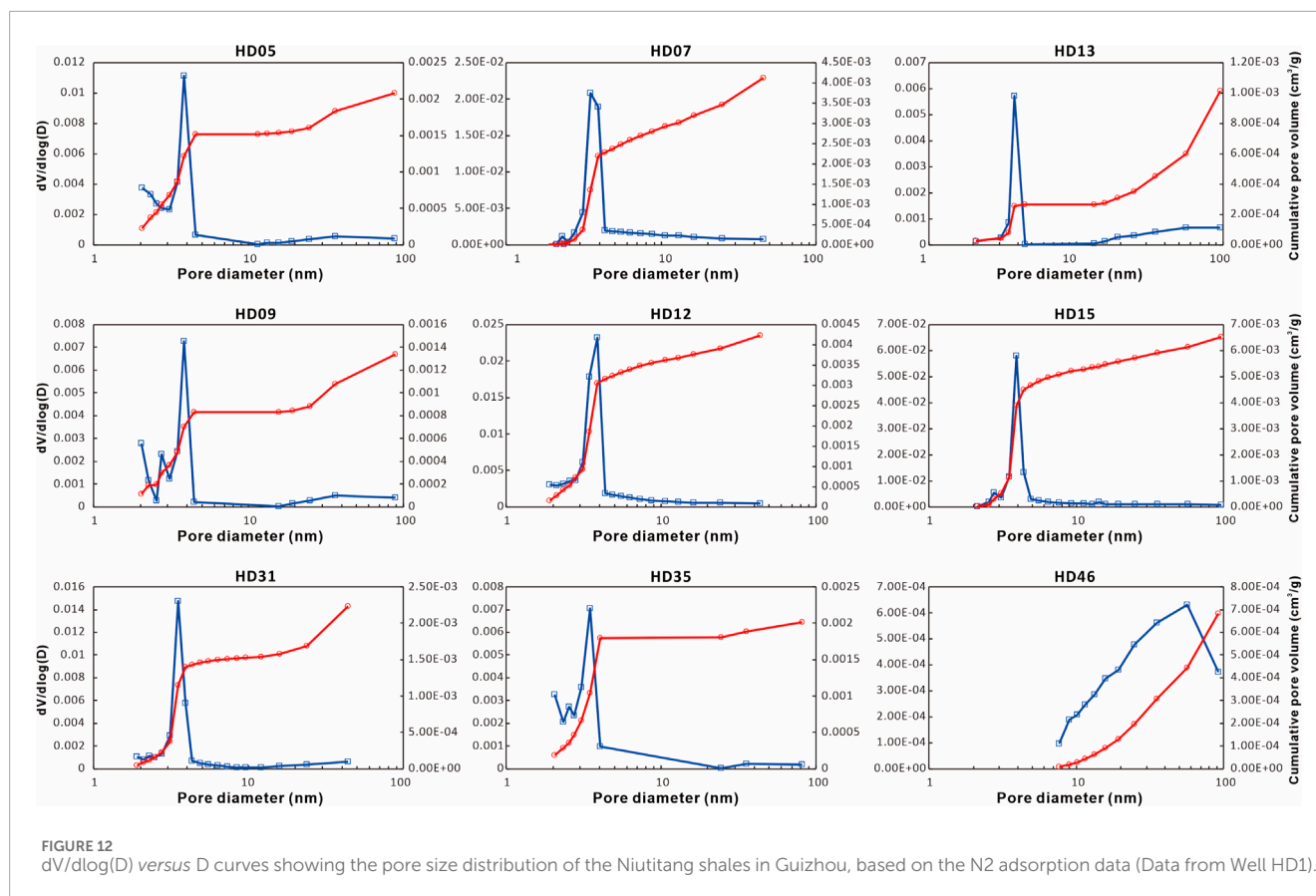


FIGURE 12 $dV/d\log(D)$ versus D curves showing the pore size distribution of the Niutitang shales in Guizhou, based on the N_2 adsorption data (Data from Well HD1).

0.634×10^{-3} to 6.52×10^{-3} cm^3/g , averaging 2.63×10^{-3} cm^3/g . The average pore diameters ranged from 2.46 to 16.81 nm, with a mean of 5.27 nm. The PSD, plotted using the BJH model on the adsorption branches, indicated a predominance of micropores and mesopores, as shown in Figure 12.

Consequently, the pore types observed in the Niutitang and Dawuba shales in Guizhou exhibit similarities, including the prevalence of inter-particle pores (Inter-P), intra-particle pores (Intra-P), organic matter pores (OM-P), and micro-fractures. The low-pressure N_2 physisorption analyses reveal a predominance of micropores and mesopores in both the Niutitang and Dawuba shales in Guizhou.

6.4 Gas contents

The gas content measurements for Dawuba shales in the Guizhou area, presented in Table 9 and illustrated in Figure 13A, reveal a range in desorbed gas content from $0.07 \text{ m}^3/\text{t}$ to $1.28 \text{ m}^3/\text{t}$, averaging at $0.46 \text{ m}^3/\text{t}$. The residual gas contents vary from $0.09 \text{ m}^3/\text{t}$ to $0.44 \text{ m}^3/\text{t}$, with an overall mean of $0.27 \text{ m}^3/\text{t}$. Notably, some samples exhibited no detectable levels of residual gas. Consequently, the total gas contents in Dawuba shales range from a minimum of $0.07 \text{ m}^3/\text{t}$ to a maximum of $1.68 \text{ m}^3/\text{t}$, with an average of $0.59 \text{ m}^3/\text{t}$.

According to the data collected from Ge et al. (2020), the Niutitang shales in the Guizhou area, as depicted in Figure 13B, demonstrate a different gas content profile. The desorbed

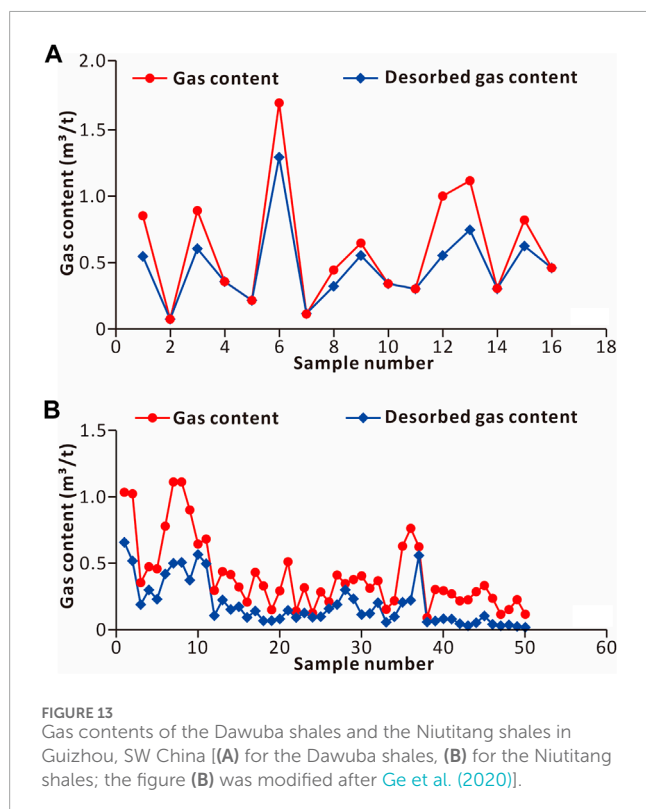
gas content for Niutitang shales ranges from $0.02 \text{ m}^3/\text{t}$ to $0.66 \text{ m}^3/\text{t}$, with an average of $0.19 \text{ m}^3/\text{t}$. The overall total shale gas content for Niutitang shales varies between $0.09 \text{ m}^3/\text{t}$ and $1.31 \text{ m}^3/\text{t}$, averaging at $0.42 \text{ m}^3/\text{t}$. These differences in gas content between the Dawuba and Niutitang shales can be attributed to variations in physical properties and preservation conditions, with the Dawuba shales generally exhibiting higher gas content levels.

7 Predicting favorable zones for shale gas

Research and practical experiences have demonstrated that the enrichment and high productivity of marine shale gas are closely linked to specific geological, engineering, and economic characteristics. These ideal conditions for shale gas extraction are often summarized as “sweet, crisp, and good,” encapsulating the essence of “good gas-bearing property” from a geological perspective, “good fracturing ability” from an engineering standpoint, and “good economic efficiency” in terms of financial benefits (Dong et al., 2016; Wang et al., 2018). Focusing on the Wufeng-Longmaxi Formations across shale gas fields such as Changning, Weiyuan, and Fuling in the Sichuan Basin, prior studies have pinpointed the critical parameters for identifying shale gas-rich sections. These parameters include the “four highs” (high Total Organic Carbon (TOC) value, high gas content, high porosity, and high formation pressure) and the “two developments”

TABLE 9 Gas contents of the Dawuba shale in Guizhou, SW China.

No.	Sample	Top depth/m	Bottom depth/m	Desorbed gas(cm ³ /g)	Loss gas (cm ³ /g)	Residual gas (cm ³ /g)	Gas content (cm ³ /g)
5-1	Shale core	2773.59	2773.71	0.54	—	0.31	0.84
5-2	Shale core	2774.58	2774.70	0.07	—	—	0.07
5-3	Shale core	2776.32	2776.42	0.60	—	0.28	0.88
5-4	Shale core	2776.84	2776.97	0.35	—	—	0.35
6-1	Shale core	2801.27	2801.41	0.21	—	—	0.21
6-2	Shale core	2800.66	2800.73	1.28	—	0.40	1.68
7-2	Shale core	2809.80	2809.89	0.10	—	—	0.10
8-1	Shale core	2884.23	2884.43	0.32	—	0.12	0.44
9-1	Shale core	2892.23	2892.33	0.55	—	0.09	0.64
9-2	Shale core	2891.00	2891.15	0.34	—	—	0.34
10-1	Shale core	2933.48	2933.56	0.30	—	—	0.30
11-1	Shale core	2942.75	2942.87	0.55	—	0.44	0.99
11-2	Shale core	2941.65	2941.84	0.74	—	0.36	1.10
12-1	Shale core	2951.66	2951.75	0.30	—	—	0.30
12-2	Shale core	2950.91	2951.06	0.62	—	0.19	0.81
13-1	Shale core	2981.00	2981.11	0.45	—	—	0.45



(well-developed shale bedding/lamination and natural microfractures) (Wang et al., 2012; Wang et al., 2013; Zhou et al., 2019). The evaluation criteria used to predict favorable exploration zones are detailed in Table 10.

Taking the Carboniferous Dawuba Formation shale in the South Guizhou Depression as a case study, this formation is characterized by its rich OM, favorable OM types, and substantial storage capacity. Previous studies have shown that hydrocarbon generation in the Dawuba shales occurred in the Late Carboniferous to Early Permian period (Chen et al., 2007). Gas generation began in the Middle to Late Permian, and hydrocarbon expulsion and migration occurred before the Middle Triassic (the Indosinian movement around 205 Ma) (Chen et al., 2007). However, the marine shale layer in southern China has undergone multiple stages of tectonic evolution (the Hercynian, Indosinian, Yanshanian, and Himalayan movements) and prolonged uplift and erosion, which have significantly influenced the target Carboniferous series. Therefore, it is imperative to consider the effects of shale self-sealing and fractures on gas preservation, as well as the impact of regional folding and denudation.

To accurately predict and optimize the most favorable areas for shale gas within the Dawuba Formation, this study utilizes a comprehensive information overlay approach. This method integrates geological benchmarks (Wang et al., 2021) for identifying favorable conditions in non-typical marine

TABLE 10 Geological reference standards for favorable areas of a non-typical marine shale gas in South China.

Parameters		Evaluation criteria for favorable areas
Shale occurrence and distribution	Area	$\geq 50 \text{ km}^2$
	Thickness	Thickness of single layer ($\geq 3 \text{ m}$), thickness of continuous layers ($\geq 10 \text{ m}$), ratio of shale to formation ($\geq 60\%$)
	Burial depth	$\geq 1,000 \text{ m}$
Geochemistry of source rock	OM Abundance	TOC $\geq 1.0 \text{ wt}\%$
	OM Thermal-maturity	$0.4\% < \text{Ro} < 4.0\%$
	OM Type	Type I-II
Shale reservoir	Mineral compositions	Contents of brittle minerals ($>45\%$)
	Gas content	$>0.5 \text{ m}^3/\text{t}$
Preservation	Fault	Undeveloped faults
	Folding	Relatively wide syncline
	Denudation	Weak denudation

The standard was modified after Wang et al. (2012) (Wang et al., 2012), Wang et al. (2013) (Wang et al., 2013), Zhou et al. (2019) (Zhou et al., 2019), and Wang et al. (2021) (Wang et al., 2021).

shales of southern China (Table 10), alongside parameters that reflect shale development conditions, source rock geochemical attributes, reservoir properties, and preservation conditions.

Data from the China Geological Survey highlight several advantageous geological features of the Carboniferous Dawuba Formation shale in the Qiannan Depression. These features include considerable thickness, widely distribution, moderate burial depth, effective OM preservation during deposition, high TOC content, predominance of type II2 kerogen, a range from high maturity to over maturity of OM, a high content of brittle minerals within the reservoir, relatively high shale gas content, and a well-developed overlying direct cap rock. In the research, we selectively focus on the TOC content, Ro values, burial depth, and shale thickness. Collectively, this comprehensive analysis identifies the Carboniferous Dawuba Formation in the Shangyuan and Zongdi areas of the Qiannan Depression as promising exploration zones for shale gas, as illustrated in Figure 14.

8 Conclusion

(1) Paleoclimate and Water Conditions: In the Upper Yangtze region, the deposition of the Carboniferous Dawuba shale took place under a warm and arid paleoclimate, with predominantly reducing water conditions that facilitated the preservation of OM. The salinity levels during this period suggested a transitional phase towards marine conditions, characterized by a shift from transitional to predominantly saline water environments. Conversely, during the Cambrian Niutitang deposition, the paleoclimate was cooler and arid, with saltwater conditions prevailing. Similar to the

Dawuba shale, reducing conditions were predominant during the Niutitang deposition, which were conducive to OM preservation.

- (2) Source Rock Potential and Organic Matter Types: The Carboniferous Dawuba shales have advanced to the post-mature stage, indicating their significant gas generation potential in ancient times, primarily due to the presence of Type II2 kerogens. Similarly, the Cambrian Niutitang shales have also reached the post-mature stage, demonstrating good to excellent gas generation potential. The dominant presence of Type I kerogens in these shales further underscores their high gas generation potential.
- (3) Shale Composition, Porosity, and Gas Content: Both the Carboniferous Dawuba and Cambrian Niutitang shales are characterized by a composition of mixed shale and argillaceous shale. These formations exhibit ultra-low porosity and permeability, yet they feature the development of dissolution pores, OM pores, and micro-fractures, which are crucial for gas storage. The Dawuba and Niutitang shales primarily contain micropores and mesopores. Comparative analysis reveals that the Dawuba shales possess superior BET-specific surface areas, total pore volumes, and average pore diameters than the Niutitang shales. However, the gas contents in both shale formations are relatively low, with average values of $0.59 \text{ m}^3/\text{t}$ for Dawuba and $0.42 \text{ m}^3/\text{t}$ for Niutitang shales. This observation highlights the need for further research to explore the conditions that favor shale gas preservation.
- (4) Prospective Exploration Areas: In Guizhou, the Qiannan Depression hosts the Carboniferous Dawuba Formation, particularly within the Shangyuan and Zongdi areas, which has emerged as promising regions for shale gas exploration. These areas exhibit favorable geological characteristics, notably

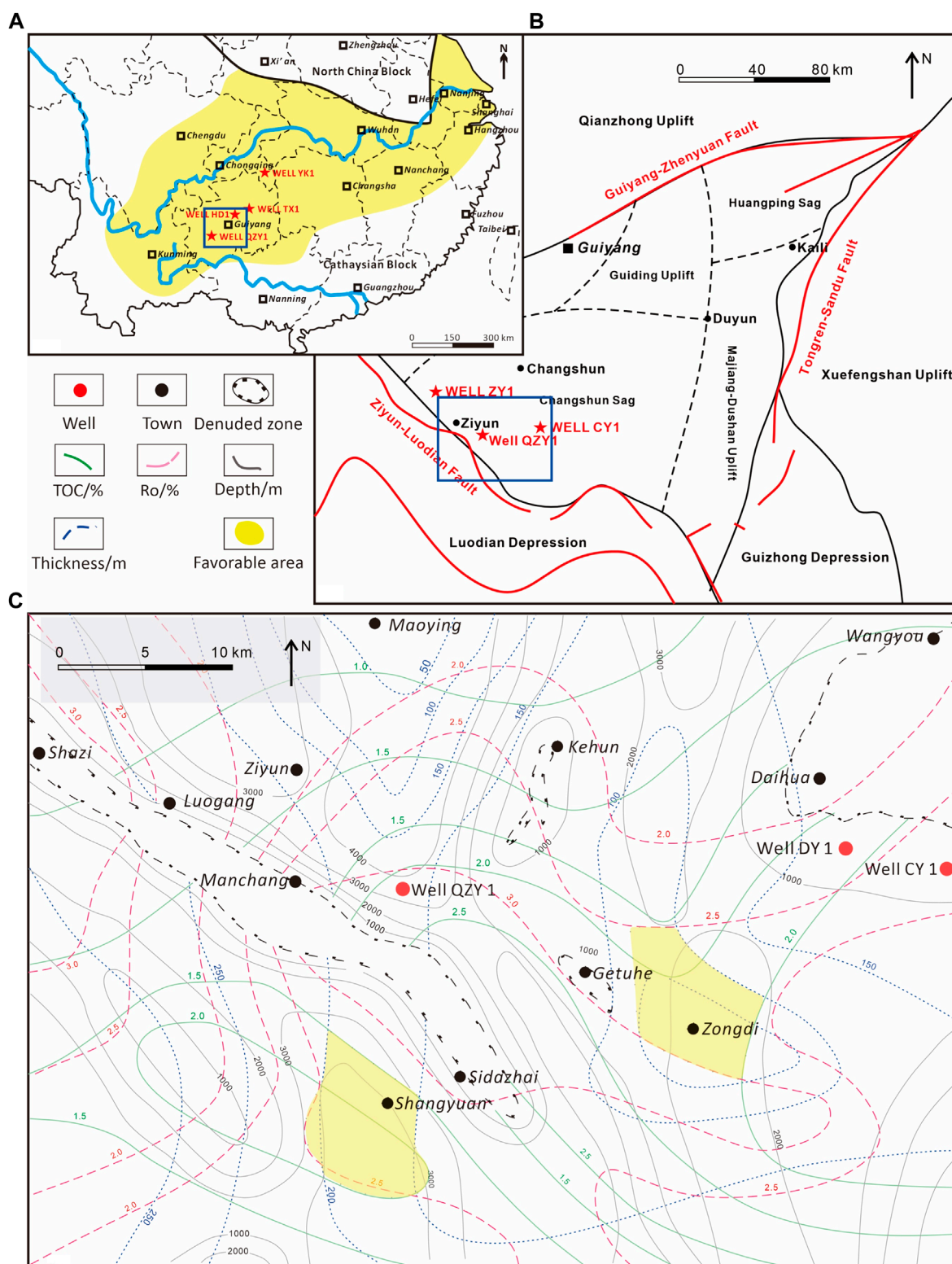


FIGURE 14 Prediction map of favorable exploration zones for shale gas in the Carboniferous Dawuba Formation of the Qiannan Depression, China [The location of figure (B) is depicted in figure (A), and the location of figure (C) is depicted within figure (B)].

high total organic carbon (TOC) and vitrinite reflectance (R_o) values, alongside moderate burial depths and shale thicknesses. These features collectively enhance the potential for significant shale gas reserves.

Data availability statement

The original contributions presented in the study are included in the article/Supplementary material, further inquiries can be directed to the corresponding author.

Author contributions

TW: Conceptualization, Methodology, Resources, Writing–review and editing. ZX: Conceptualization, Funding acquisition, Methodology, Writing–original draft. KY: Data curation, Methodology, Resources, Writing–review and editing. XW: Conceptualization, Supervision, Writing–review and editing, Resources. MG: Writing–review and editing, Data curation, Formal Analysis, Resources.

Funding

The author(s) declare that financial support was received for the research, authorship, and/or publication of this article. The Natural Science Foundation of Chongqing [No. cstc2021jcyj-msxmX0733], the China Geological Survey Projects of Strategic Selection of Upper Paleozoic Shale Gas in the Yunnan-Guizhou-Guangxi Region [No. DD20160196], the Shale Gas Survey in the Guizhong-Nanpanjiang Area [No. DD20190088], the Science and Technology Innovation Project of Oil and Gas Survey, China Geological Survey [No. 2023YC08], the Open Fund of Key Laboratory of Sedimentary Basins and Oil and Gas Resources,

Ministry of Natural Resources [No. cdcgs2022006, cdcgs2023009], the Science and Technology Research Program of Chongqing Municipal Education Commission [No. KJQN202101530], the China Postdoctoral Science Foundation [No. 2023MD734109], the Open Fund of Key Laboratory of Tectonics and Petroleum Resources (China University of Geosciences), Ministry of Education (No. TPR-2023-06), and the College Students' Innovative Entrepreneurial Training Plan Program of CQUST [No. 2023151]. Their support has been instrumental in the successful completion of this research project.

Acknowledgments

The authors would like to express their sincere gratitude to the Oil and Gas Survey, China Geological Survey for providing the necessary data and granting permission to publish the results of this study.

Conflict of interest

The authors declare that the research was conducted in the absence of any commercial or financial relationships that could be construed as a potential conflict of interest.

Publisher's note

All claims expressed in this article are solely those of the authors and do not necessarily represent those of their affiliated organizations, or those of the publisher, the editors and the reviewers. Any product that may be evaluated in this article, or claim that may be made by its manufacturer, is not guaranteed or endorsed by the publisher.

References

- Adegoke, A. K., Abdullah, W. H., Hakimi, M. H., and Sarki Yandoka, B. M. (2014). Geochemical characterisation of Fika Formation in the Chad (Bornu) Basin, northeastern Nigeria: implications for depositional environment and tectonic setting. *Appl. Geochem.* 43, 1–12. doi:10.1016/j.apgeochem.2014.01.008
- Algeo, T. J., and Lyons, T. W. (2022). Mo-total organic carbon covariation in modern anoxic marine environments: implications for analysis of paleoredox and paleohydrographic conditions. *Paleoceanography* 21, PA1016. doi:10.1029/2004pa001112
- Ayinla, H. A., Wan, H. A., Makeen, Y. M., Abubabar, M., Jauro, A., Mohammed, B., et al. (2017). Petrographic and geochemical characterization of the Upper Cretaceous coal and mudstones of Gombe Formation, Gongola sub-basin, northern Benue trough Nigeria: implication for organic matter preservation, paleodepositional environment and tectonic settings. *Int. J. Coal Geol.* 180, 67–82. doi:10.1016/j.coal.2017.06.010
- Bai, Y., Liu, Z., Sun, P., Liu, R., Hu, X., Zhao, H., et al. (2015). Rare earth and major element geochemistry of Eocene fine-grained sediments in oil shale- and coal bearing layers of the Meihe Basin, northeast China. *J. Asian Earth Sci.* 97, 89–101. doi:10.1016/j.jseas.2014.10.008
- Barrett, E. P., Joyner, L. G., and Halenda, P. P. (1951). The determination of pore volume and area distributions in porous substances. I. Computations from nitrogen isotherms. *J. Am. Chem. Soc.* 73 (1), 373–380. doi:10.1021/ja01145a126
- Blatt, H. (1982). *Sedimentary petrology*. Oxford: Freeman and Company, Ltd.,
- Boggs, S. (2006). *Principles of sedimentology and stratigraphy*. London: Pearson Prentice Hall.
- Bordenave, M. L., Espitalié, L., Leplat, P., Oudin, J. L., and Vandenbroucke, M. (1993). "Screening techniques for source rock evaluation." in *Applied petroleum Geochemistry*. Editor M. L. Bordenave (Paris: Editions Technip).
- Chen, D., Wang, J., Qing, H., Yan, D., and Li, R. (2009). Hydrothermal venting activities in the Early Cambrian, south China: petrological, geochronological and stable isotopic constraints. *Chem. Geol.* 258, 168–181. doi:10.1016/j.chemgeo.2008.10.016
- Chen, Y. Z., Liu, L. F., Cai, X. Y., and Wang, Y. (2007). An analysis of hydrocarbon reservoir conditions of Late Paleozoic marine strata in South China. *Nat. Gas. Ind.* 27 (10), 20–23.
- Clarkson, C. R., Solano, N., Bustin, R. M., Bustin, A. M. M., Chalmers, G. R. L., He, L., et al. (2013). Pore structure characterization of North American shale gas reservoirs using USANS/SANS, gas adsorption, and mercury intrusion. *Fuel* 103, 606–616. doi:10.1016/j.fuel.2012.06.119
- Couture, R. A., Smith, M. S., and Dymek, R. F. (1993). X-ray fluorescence analysis of silicate rocks using fused glass discs and a side-window Rh source tube: accuracy, precision and reproducibility. *Chem. Geol.* 110 (4), 315–328. doi:10.1016/0009-2541(93)90326-e
- Curtis, J. B. (2002). Fractured shale-gas systems. *AAPG Bull.* 86, 1921–1938. doi:10.1306/61eedd8e-173e-11d7-8645000102c1865d

- Dong, D. Z., Wang, Y. M., Huang, X. N., Zhang, C. C., Guan, Q. Z., Huang, J. L., et al. (2016). Discussion about geological characteristics, resource evaluation methods and its key parameters of shale gas in China. *Nat. Gas. Geosci.* 27 (9), 1583–1601.
- Durand, B., and Nicaise, G. (1980). "Procedures for kerogen isolation," in *kerogen: insoluble organic matter from sedimentary rocks*. Editor B. Durand (Paris: Editions Technip).
- Espalitie, J., LaPorte, J. L., Madec, M., Marquis, F., LePlat, P., Paulet, J., et al. (1977). Méthode rapide de caractérisation des roches mères, de leur potentiel pétrolier et de leur degré d'évolution. *Oil Gas. Sci. Technol.* 32, 23–42. doi:10.2516/ogst:1977002
- Garrels, R. M., and Mackenzie, F. T. (1969). Sedimentary rock types: relative proportions as a function of geological time. *Science* 163 (3867), 570–571. doi:10.1126/science.163.3867.570
- Ge, M. N., Bao, S. J., Shi, D. S., Ma, Y., Zhang, J. C., Zhang, Q., et al. (2024). Multi-scale characterization of shale pore structure of Niutitang Formation in southeastern Guizhou and its influence on shale gas enrichment. *Geol. China* 51 (01), 57–72.
- Ge, M. N., Chen, K., Chen, L. X., Wang, C., and Bao, S. J. (2020). The influence factors of gas-bearing and geological characteristics of Niutitang Formation shale in the southern margin of Xuefeng Mountain anticline uplift: a case of Well Huangdi 1. *China Geol.* 3, 533–544. doi:10.31035/cg2020072
- Goldberg, T., Strauss, H., Guo, Q., and Liu, C. (2007). Reconstructing marine redox conditions for the Early Cambrian Yangtze Platform: evidence from biogenic sulphur and organic carbon isotopes. *Paleogeogr. Palaeoclimatol. Palaeoecol.* 254, 175–193. doi:10.1016/j.palaeo.2007.03.015
- Guizhou Geological Survey Institute (2017). *Regional geology of China, Guizhou province*. Beijing: Geological Publishing House, 1153.
- Guo, R. L., Zhao, Y. D., Wang, W. B., Hu, X. Y., Zhou, X. P., Hao, L. W., et al. (2020). Application of rare-earth elements and comparison to molecular markers in oil-source correlation of tight oil: a case study of Chang 7 of the Upper Triassic Yanchang Formation in Longdong area, Ordos Basin, China. *ACS Omega* 5, 22140–22156. doi:10.1021/acsomega.0c02233
- Hakimi, M. H., Abdullah, W. H., and Shalaby, M. R. (2011). Organic geochemical characteristics of crude oils from the Masila Basin, eastern Yemen. *Org. Geochem.* 42, 465–476. doi:10.1016/j.orggeochem.2011.03.015
- Hatch, J. R., and Leventhal, J. S. (1992). Relationship between inferred redox potential of the depositional environment and geochemistry of the Upper Pennsylvanian (Missourian) Stark Shale Member of the Dennis Limestone, Wabaunsee County, Kansas, U.S.A. *Chem. Geol.* 99, 65–82. doi:10.1016/0009-2541(92)90031-y
- Hu, T., Pang, X. Q., Xu, T. W., Li, C. R., Jiang, S., Wang, Q., et al. (2022). Identifying the key source rocks in heterogeneous saline lacustrine shales: Paleogene shales in the Dongpu depression, Bohai Bay Basin, eastern China. *AAPG Bull.* 106 (6), 1325–1356. doi:10.1306/01202218109
- Jarvie, D. M., Hill, R. J., Ruble, T. E., and Pollastro, R. M. (2007). Unconventional shale-gas systems: the Mississippian Barnett Shale of north-central Texas as one model for thermogenic shale-gas assessment. *AAPG Bull.* 91, 475–499. doi:10.1306/12190606068
- Jenner, G. A., Longerich, H. P., Jackson, S. E., and Fryer, B. J. (1990). ICP-MS-A powerful tool for high-precision trace-element analysis in earth sciences: evidence from analysis of selected U.S.G.S. reference samples. *Chem. Geol.* 83, 133–148. doi:10.1016/0009-2541(90)90145-w
- Jin, L. X., Ogrinc, N., Yesavage, T., Hasenmueller, E. A., Ma, L., Sullivan, P. L., et al. (2014). The CO₂ consumption potential during gray shale weathering: insights from the evolution of carbon isotopes in the Susquehanna Shale Hills critical zone observatory. *Geochim. Cosmochim. Acta* 142, 260–280. doi:10.1016/j.gca.2014.07.006
- Jones, B., and Manning, D. A. C. (1994). Comparison of geochemical indices used for the interpretation of palaeoredox conditions in ancient mudstones. *Chem. Geol.* 111, 111–129. doi:10.1016/0009-2541(94)90085-x
- Kaiser, S. I., Becker, R. T., Steuber, T., and Aboussalam, S. Z. (2011). Climate-controlled mass extinctions, facies, and sea-level changes around the Devonian–Carboniferous boundary in the eastern Anti-Atlas (SE Morocco). *Paleogeogr. Palaeoclimatol. Palaeoecol.* 310, 340–364. doi:10.1016/j.palaeo.2011.07.026
- Kirschvink, J. L. (1992). *A paleogeographic model for vendian and cambrian time, the proterozoic biosphere: a multidisciplinary study*. New York: Cambridge University Press, 567–581.
- Kuila, U., and Prasad, M. (2013). Specific surface area and pore-size distribution in clays and shales. *Geophys Prospect* 61 (2), 341–362. doi:10.1111/1365-2478.12028
- Lakin, J. A., Marshall, J. E. A., Troth, I., and Harding, I. C. (2016). "Greenhouse to icehouse: a biostratigraphic review of latest Devonian–Mississippian glaciations and their global effects," in *Devonian climate, sea level and evolutionary events*. Editors R. T. Becker, P. K. Onigshof, and C. E. Brett (London: Special Publications. Geological Society), 439–464.
- Lerman, A. D. I., and Gat, J. (1989). *Physics and chemistry of lakes*. Berlin: Springer-Verlag.
- Li, Y. F., Fan, T. L., Zhang, J. C., Zhang, J. P., Wei, X. J., Hu, X. L., et al. (2015). Geochemical changes in the Early Cambrian interval of the Yangtze Platform, South China: Implications for hydrothermal influences and paleocean redox conditions. *J. Asian Earth Sci.* 109, 100–123. doi:10.1016/j.jseas.2015.05.003
- Lin, Z. J., Chen, D. F., and Liu, Q. (2008). Geochemical indices for redox conditions of marine sediments. *Bull. China Soc. Mineral. Petrol. Geochem.* 27 (1), 72–80.
- Liu, J. S., Algeo, T. J., Qie, W. K., and Saltzman, M. R. (2019). Intensified oceanic circulation during early Carboniferous cooling events: evidence from carbon and nitrogen isotopes. *Paleogeogr. Paleoclimatol. Paleoecol.* 531, 108962. doi:10.1016/j.palaeo.2018.10.021
- López, L., Lo Monaco, S., Galarraga, E., Lira, A., and Cruz, C. (1995). V/Ni ratio in maltene and asphaltene fractions of crude oils from the west Venezuelan basin: correlation studies. *Chem. Geol.* 119, 255–262. doi:10.1016/0009-2541(94)00100-m
- Lowell, S., Shields, J. E., Thomas, M. A., and Thommes, M. (2004). *Characterization of porous solids and powders: surface area, pore size and density*. Berlin, Germany: Springer.
- Lu, S. F. (2019). *Study on shale gas accumulation rules and exploration area of Dawuba Formation of Carboniferous in Guizhou Province*. Guiyang, China: Guizhou University.
- Ma, F. H., Pan, J. L., Ma, R. Y., Zhang, Y., and Ma, X. J. (2019). Division of immature mud-shale organic type of Madongshan Formation in Liupanshan Basin. *Nat. Gas. Geosci.* 30, 1370–1377.
- Ma, Y., Zhong, N. N., Cheng, L. J., Pan, Z. J., Li, H. Y., Xie, Q. M., et al. (2015). Pore structure of two organic-rich shales in southeastern Chongqing area: Insight from Focused Ion Beam Scanning Electron Microscope (FIB-EM). *Petroleum Geol. Exp.* 37 (1), 109–116.
- Meert, J. G. (2003). A synopsis of events related to the assembly of eastern Gondwana. *Tectonophysics* 362, 1–40. doi:10.1016/s0040-1951(02)00629-7
- Meng, Q. T., Liu, Z. J., Bruch, A. A., Liu, R., and Hu, F. (2012). Palaeoclimatic evolution during Eocene and its influence on oil shale mineralisation, Fushun basin, China. *J. Asian Earth Sci.* 45, 95–105. doi:10.1016/j.jseas.2011.09.021
- Milliken, K. A. (2014). A Compositional Classification For Grain Assemblages In Fine-Grained Sediments and Sedimentary Rocks. *J. Sediment. Res.* 84 (12), 1185–1199. doi:10.2110/jsr.2014.92
- Mongenot, T., Tribouillard, N., Desprairies, A., Lallier-Vergès, E., and Laggoun-Defarge, F. (1996). Trace elements as palaeoenvironmental markers in strongly mature hydrocarbon source rocks: the Cretaceous La Luna Formation of Venezuela. *Sediment. Geol.* 103, 23–37. doi:10.1016/0037-0738(95)00078-x
- Mukhopadhyay, P. K., Wade, J. A., and Kruger, M. A. (1995). Organic facies and maturation of Jurassic/Cretaceous rocks, and possible oil source rock correlation based on pyrolysis of asphaltene, Scotian Basin, Canada. *Org. Geochem.* 22, 85–104. doi:10.1016/0146-6380(94)00061-1
- Peters, K. E., and Cassa, M. R. (1994). "Applied source rock geochemistry," in *The petroleum system-from source to trap*. Editors L. B. Magoon, L. B. Magoon, and W. G. Dow (Tulsa, OK: AAPG Memoir), 93–120.
- Qie, W. K., Algeo, T. J., Luo, G. M., and Herrmann, A. (2019). Global events of the late Palaeozoic (early Devonian to Middle Permian): a review. *Paleogeogr. Palaeoclimatol. Palaeoecol.* 531, 109259. doi:10.1016/j.palaeo.2019.109259
- Ross, D. J. K., and Bustin, R. M. (2006). Sediment Geochemistry of the Lower Jurassic Gordondale Member, Northeastern British Columbia. *Bull. Can. Petroleum Geol.* 54 (4), 337–365. doi:10.2113/gscpgbull.54.4.337
- Sarki Yandoka, B. M., Abdullah, W. H., Abubakar, M. B., Hakimi, M. H., and Adegoke, A. K. (2015). Geochemical characterisation of Early Cretaceous lacustrine sediments of Bima Formation, Yola Sub-basin, Northern Benue Trough, NE Nigeria: Organic matter input, preservation, paleoenvironment and palaeoclimatic conditions. *Mar. Petrol. Geol.* 61, 82–94. doi:10.1016/j.marpetgeo.2014.12.010
- Sing, K. S. (1995). Physisorption of nitrogen by porous materials. *Mater* 2 (1), 5–8. doi:10.1007/bf00486564
- Steiner, M., Wallis, E., Erdtmann, B. D., Zhao, Y. L., and Yang, R. D. (2001). Submarine hydrothermal exhalative ore layers in black shales from South China and associated fossils – insights into a Lower Cambrian facies and bio-evolution. *Paleogeogr. Palaeoclimatol. Palaeoecol.* 169, 165–191. doi:10.1016/s0031-0182(01)00208-5
- Suleimenova, A., Bake, K. D., Ozkan, A., Valenza, J. J., Kleinberg, R. L., Burnham, A. K., et al. (2014). Acid demineralization with critical point drying: a method for kerogen isolation that preserves microstructure. *Fuel* 135, 492–497. doi:10.1016/j.fuel.2014.07.005
- Tan, J., Horsfield, B., Fink, R., Krooss, B., Schulz, H., Rybacki, E., et al. (2014). Shale gas potential of the major marine shale formations in the Upper Yangtze Platform, South China, part III: mineralogical, lithofacial, petrophysical, and rock mechanical properties. *Energy Fuels* 28, 2322–2342. doi:10.1021/ef4022703
- Tan, J., Horsfield, B., Mahlstedt, N., Zhang, J., Boreham, C., Hippler, D., et al. (2015). Natural gas potential of Neoproterozoic and lower Palaeozoic marine shales in the Upper Yangtze Platform, South China: geological and organic geochemical characterization. *Int. Geol. Rev.* 57 (3), 305–326. doi:10.1080/00206814.2015.1004200
- Tan, J., Horsfield, B., Mahlstedt, N., Zhang, J., Diprimio, R., Vu, T., et al. (2013). Physical properties of petroleum formed during maturation of Lower Cambrian shale in the upper Yangtze Platform, South China, as inferred from PhaseKinetics modelling. *Mar. Petrol. Geol.* 48, 47–56. doi:10.1016/j.marpetgeo.2013.07.013
- Tissot, B. P., and Welte, D. H. (1984). *Petroleum Formation and occurrence*. Berlin: Springer-Verlag.

- Wang, J. Z., Li, X. G., Xu, Z. J., Xin, Y. L., Li, Z., and Li, Y. W. (2021). Shale Gas Accumulation Conditions and Favorable-zone prediction in the Lower Carboniferous Luzhai Formation in Donglan Area of the Nanpanjiang Depression, China. *Earth Sci.* 46 (5), 1814–1828.
- Wang, L. (2020). *Enrichment conditions and recoverable resources of shale gas of the focus layers in southeast Chongqing*. Beijing, China: China University of Geosciences Beijing.
- Wang, P. F., Jiang, Z. X., Chen, L., Yin, L. S., Li, Z., Zhang, C., et al. (2016). Pore structure characterization for the Longmaxi and Niutitang shales in the Upper Yangtze Platform, South China: Evidence from focused ion beam-He ion microscopy, nano-computerized tomography and gas adsorption analysis. *Mar. Pet. Geol.* 77, 1323–1337.
- Wang, P. F., Jiang, Z. X., Han, B., Lv, P., Jin, C., Zhang, K., et al. (2018). Reservoir Geological Parameters for Efficient Exploration and Development of Lower Cambrian Niutitang Formation Shale Gas in South China. *Acta Pet. Sin.* 39 (2), 152–162.
- Wang, Q. F., Yang, L., Xu, X. J., Santosh, M., Wang, Y. N., Wang, T. Y., et al. (2020a). Multi-stage tectonics and metallogeny associated with Phanerozoic evolution of the South China Block: a holistic perspective from the Youjiang Basin. *Earth-Sci. Rev.* 211, 103405. doi:10.1016/j.earscirev.2020.103405
- Wang, S. J., Yang, T., Zhang, G. S., Li, D. H., and Chen, X. M. (2012). Shale gas enrichment factors and the selection and evaluation of the core area. *Strategic Study CAE* 14 (6), 94–100.
- Wang, S. Q., Wang, S. Y., Man, L., Dong, D. Z., and Wang, Y. M. (2013). Appraisal method and key parameters for screening shale gas play. *J. Chengdu Univ. Technol. Sci. Technol. Ed.* 40 (6), 609–620.
- Wang, S. Y., Zhang, H., Wang, T. H., Wang, C. H., Peng, C. L., Hu, R. F., et al. (2006). Filling and evolution of the late Paleozoic Shuicheng-Ziyun aulacogen in western Guizhou, China. *Geol. Bull. China* 25, 402–407. (in Chinese with English abstract).
- Wang, X. D., Hu, K. Y., Qie, W. K., Sheng, Q. Y., Chen, B., Lin, W., et al. (2019b). Carboniferous integrative stratigraphy and timescale of China. *Sci. China Earth Sci.* 62, 135–153. doi:10.1007/s11430-017-9253-7
- Wang, X. F., Peng, J., Yu, L. D., and Xu, T. Y. (2020b). A review of the research methods of paleosalinity geochemistry in continental strata. *Sichuan Geol. J.* 40 (2), 301–308.
- Wang, X. X., Hou, J. G., Li, S. H., Dou, L. X., Song, S. H., Kang, Q. Q., et al. (2019a). Insight into the nanoscale pore structure of organic-rich shales in the Bakken Formation, USA. *J. Petroleum Sci. Eng.* 176, 312–320.
- Wang, Y., and Cheng, H. F. (2023). Advances in microscopic pore structure characterization of fine-grained mudrocks. *Energy fuels.* 37 (3), 1495–1510. doi:10.1021/acs.energyfuels.2c03144
- Wang, Y., Cheng, H. F., Hu, Q. H., Jia, L. B., Wang, X. M., Gao, S. S., et al. (2023). Adsorption of methane onto mudstones under supercritical conditions: Mechanisms, physical properties and thermodynamic parameters. *Petrol. Sci.* 20 (1), 34–47. doi:10.1016/j.petsci.2022.08.017
- Wedepohl, K. H. (1971). Environmental influences on the chemical composition of shales and clays. *Phys. Chem. Earth* 8, 307–333. doi:10.1016/0079-1946(71)90020-6
- Wright, J., Schrader, H., and Holser, W. T. (1987). Paleoredox variations in ancient oceans recorded by rare earth elements in fossil apatite. *Geochem Cosmochim. Acta* 51 (3), 631–644. doi:10.1016/0016-7037(87)90075-5
- Wu, C. J., Tuo, J. C., Zhang, M. F., Sun, L. N., Yu, Q., and Liu, Y. (2016). Sedimentary and residual gas geochemical characteristics of the Lower Cambrian organic-rich shales in Southeastern Chongqing, China. *Mar. Petroleum Geol.* 75, 140–150. doi:10.1016/j.marpetgeo.2016.04.013
- Wu, G. Y., Wang, W. F., and Chi, H. X. (2012). Basin evolution and later reformation of marine sediments in southern Guizhou Depression and neighboring areas. *J. Palaeogeography* 14 (4), 507–521.
- Xu, Z. J., Li, X. G., Li, J., Xue, Y. L., Jiang, S., Liu, L. F., et al. (2022b). Characteristics of Source Rocks and Genetic Origins of Natural Gas in Deep Formations, Gudian Depression, Songliao Basin, NE China. *ACS Earth Space Chem.* 6 (7), 1750–1771. doi:10.1021/acsearthspacechem.2c00065
- Xu, Z. J., Liu, L. F., Liu, B. J. M., Wang, T. G., Zhang, Z. H., Wu, K. J., et al. (2019). Geochemical characteristics of the Triassic Chang 7 lacustrine source rocks, Ordos Basin, China: Implications for paleoenvironment, petroleum potential and tight oil occurrence. *J. Asian Earth Sci.* 178, 112–138. doi:10.1016/j.jseas.2018.03.005
- Xu, Z. J., Wang, Y., Jiang, S., Fang, C., Liu, L. F., Wu, K. J., et al. (2022a). Impact of input, preservation and dilution on organic matter enrichment in lacustrine rift basin: A case study of lacustrine shale in Dehui Depression of Songliao Basin, NE China. *Mar. Petr. Geol.* 135, 105386. doi:10.1016/j.marpetgeo.2021.105386
- Yang, X., Lei, Y., Zhang, J. C., Chen, S. J., Chen, L. Q., Zhong, K. S., et al. (2021). Depositional environment of shales and enrichment of organic matters of the Lower Cambrian Niutitang Formation in the Upper Yangtze Region. *Nat. Gas. Ind. B* 8, 666–679. doi:10.1016/j.ngib.2021.11.001
- Yuan, K., Wang, K. Y., Gong, S. H., Qin, Y. L., Lu, S. F., Chen, R., et al. (2018). Shale Gas Enrichment Features and Impacting Factors in Carboniferous Dawuba Formation, Southern Guizhou Area. *Coal Geol. China* 30, 28–34.
- Zeng, S. Q., Wang, J., Fu, X. G., Chen, W. B., Feng, X. L., Wang, D., et al. (2015). Geochemical characteristics, redox conditions, and organic matter accumulation of marine oil shale from the Changliang Mountain area, northern Tibet, China. *China. Mar. Petrol. Geol.* 64, 203–221. doi:10.1016/j.marpetgeo.2015.02.031
- Zeng, Y. H., Fu, X. G., Zeng, S. Q., and Du, G. (2013). Upper Triassic potential source rocks in the Qiangtang Basin, Tibet: organic geochemical characteristics. *J. Pet. Geol.* 36, 237–255. doi:10.1111/jpg.12554
- Zhang, L. T. (2019). *Geochemical characteristics and geological significance of organic-rich shale in Chongqing area*. Beijing, China: China University of Geosciences Beijing.
- Zhang, Y. Y., He, Z. L., Gao, B., and Liu, Z. B. (2017). Sedimentary environment of the Lower Cambrian organic-rich shale and its influence on organic content in the Upper Yangtze. *Pet. Geol. Exp.* 39 (2), 154–161.
- Zhou, W., Jiang, Z. X., Qiu, H. Y., Jin, X. C., Wang, R. H., Cen, W. P., et al. (2019). Shale Gas Accumulation Conditions and Prediction of Favorable Areas for the Lower Carboniferous Luzhai Formation in Guizhong Depression. *Acta Pet. Sin.* 40 (7), 798–812.
- Zou, C. N., Zhu, R. K., Dong, D. Z., and Wu, S. T. (2022). Scientific and technological progress, development strategy and policy suggestion regarding shale oil and gas. *Acta Pet. Sin.* 43 (12), 1675–1686.